

Belgian Institute for Space Aeronomy  
Department “*Atmospheres*”  
Section “*Sources and Sinks*”  
Avenue Circulaire 3, B-1180  
Brussels, Belgium



Brussels, 10 September 2015

Dear Editor,

In the current version of our manuscript we have addressed the comments and technical corrections suggested by the reviewers. Please find hereafter the list of main changes and the replies to the reviewers' comments. I hope that you will find the present version of the paper suitable for publication in *Atmospheric Chemistry and Physics*. We would like to thank you again for your consideration.

Yours sincerely,

Dr. Trissevgeni Stavrakou  
Belgian Institute for Space Aeronomy  
Avenue Circulaire, 3, 1180  
Brussels, Belgium  
Trissevgeni.Stavrakou@aeronomie.be

### List of main changes

- A new table is added (Table 1 of the revised version) summarizing all forward sensitivity simulations used to investigate the diurnal variation of HCHO columns. The table is introduced in the first paragraph of Section 3.1.
- We followed the suggestion of Reviewer#2 and moved Section 2.2 in the Supplement. Its content is briefly presented in Section 2.
- A new section “Inversion methodology” (Section 5) has been added with information on the technique and material from the section “Overview of the results” of the first version of the manuscript.
- We added information about the global budget of HCHO (last paragraph of Section 2).
- Additional references and discussion have been inserted in the introduction of the revised version.
- More detailed information about the IMAGESv2 CTM is presented in Section 2.
- Section 7.2 and 8.3, on Russian and Indochinese fluxes, respectively, are enriched to comply with the reviewers’ comments.

## Reply to Reviewer#1 comments

The authors would like to thank Reviewer#1 for the positive evaluation of the manuscript, the careful reading and the useful comments and suggestions. Below we address the raised concerns. The reviewer's comments are *italicized*.

*Stavrakou et al. utilize GOME-2 and OMI HCHO columns in an inversion with the adjoint of the IMAGESv2 CTM to evaluate the consistency of a posteriori emissions derived from the two different satellite sensors for anthropogenic, biogenic, and biomass burning VOCs. There was a good degree of consistency between the results obtained for biogenic and biomass burning emissions, with some interesting regional differences. Impacts of specific events such as Russian fires and Amazonian drought are discussed. This work is useful in the context of several recent studies that have used one or more satellite HCHO products to estimate biogenic and/or biomass burning emissions of VOCs. It is generally well-written (though a bit cumbersome to read at times, see comments below) and the scope is certainly appropriate for ACP. I recommend publication after the following comments are addressed.*

*General comments:*

- 1. Since monthly averages are used in the inversion, it would be good to know how the variation in frequency of retrievals between the two sensors (due to cloud cover, etc.) is handled in the cost function. Differences in coverage are touched on a bit in the results sections (specifically with regards to solar zenith angle and cloud cover), which is helpful information that could be expanded upon. Are there any systematic differences between the two sensors that could be introduced in Section 4?*

We have now clarified the handling of retrieval frequency (in Section 4): “The simulated monthly averaged columns are calculated from daily values weighted by the number of satellite (OMI or GOME-2) measurements for each day at each model grid cell.” It follows that the variation in frequency of retrievals between the two sensors is taken into account.

- 2. What are the implications of including isoprene as the only biogenic VOC in the a priori emissions? It seems like the seasonality of satellite-retrieved HCHO in some regions (particularly in the U.S.) is such that it peaks sooner in the summer than the model HCHO. Could this be due to the impact of VOCs that have earlier springtime emissions, such as methanol?*

Isoprene is actually not the only biogenic VOC included in the model and we apologize for not providing information on non-isoprene BVOCs. The model description has been expanded with the following text: “Monthly averaged biogenic methanol emissions (100 Tg/year globally) are taken from a previous inverse modelling study (Stavrakou et al., 2011) using IMAGESv2 and methanol total columns from IASI. Biogenic emissions of acetaldehyde (22 Tg/year) and ethanol (22 Tg/year) are calculated following Millet et al. (2010). The model also includes the biogenic emissions of ethene, propene, formaldehyde, acetone and monoterpenes from MEGANv2 (<http://eccad.sedoo.fr/>). Note that the non-isoprene biogenic VOC emissions are not varied in the source inversions.”

Varying methanol emissions along with isoprene would not seem appropriate given the direct constraints provided by IASI methanol observations.

- 3. It is difficult to navigate the discussion in Sections 6 and 7 with so many figures to flip back and forth through, particularly in regards to the discussions on biomass burning. You mention*

biomass burning results for the North China Plain for June, a month which is not included in Fig. 9, so you have also included the timelines of fluxes for different regions in Fig. 12. Is there any way to combine or condense this a bit? Also, some of the navigation would be helped if the text more explicitly referred to what aspect of a particular figure illustrates the point being made (i.e. rather than making a statement that ends with a reference to Fig. X in parentheses, I would start more statements like “The data for region Z in Fig. X show...”).

Although we agree with the referee that the discussion might appear long and sometimes difficult to follow, we do not believe practical (nor desirable) to combine or condense the different figures presenting the emission updates. Whereas Figs. 9–11 present the geographical distributions of the updates for the standard (OMI and GOME-2) inversions, the Figs. 12–13 present seasonal variations of the emissions, not only for the standard simulations but also for the different sensitivity inversions. However, to avoid confusion, the text has been amended where appropriate to make more precise references to the figures, as suggested by the referee.

*Specific comments:*

1. Page 12024, Line 12: Is there any justification to be provided for the a priori uncertainty values used?

The error values are chosen so as to reflect the higher uncertainty associated with the fire source (factor of 3) and biogenic emissions (factor of 2). The error in anthropogenic emissions for OECD countries is assumed to be lower (1.5) than for other countries. We acknowledge that these values are somewhat arbitrary, and this is the reason why we present sensitivity inversions assuming either doubled or halved a priori errors (Table 2).

2. Page 12026, Line 2: What numbers are being referred to here? The global ones? Looking at Table 3, OMI-HE corresponds to a 8% decrease from the a priori isoprene emissions, whereas OMI-DE corresponds to a 16% decrease. Correct? It would be odd if both produced larger isoprene reductions than the standard OMI inversion (~13%).

It is now mentioned that the numbers are total estimates. As the reviewer points out, the standard OMI inversion leads to a decrease of 13% with respect to the a priori, whereas OMI-HE and OMI-DE produce a decrease of 8% and 16%, respectively.

3. Page 12027, Line 19: Here it mentions that Fig. 14 contains a posteriori results for both the OMI and GOME-2 inversion, but only the OMI results are shown.

The reviewer is right. The resulting modelled GOME-2 and OMI HCHO mixing ratio are very similar. We show only OMI-derived results in Figure 14 for the sake of simplicity.

4. Page 12028, Line 12: How do we know this is not just a conflation of the isoprene and biomass burning emissions? It seems the isoprene increase in the OMI inversion is highly correlated spatially with the biomass burning emission increase (though different months are shown), whereas a posteriori isoprene over the rest of Europe is reduced relative to the a priori (in the GOME-2 inversion at least).

The referee raises a valid point. The discussion has been expanded as follows: “Note that, although the isoprene enhancement over Russia peaks earlier (July) and at slightly higher latitudes (ca. 61° N) than the biomass burning emission enhancement (55–57° N in August), the

significant overlap of the two distributions makes impossible to rule out that pyrogenic emissions are the only cause for the observed strong formaldehyde columns. The very widespread extent of the observed formaldehyde plume cannot be easily explained by the comparatively much more localized emissions of the GFED3 inventory, and an additional, more widespread formaldehyde source (such as isoprene) could help to explain the observations. However, as discussed below, the GFED3 total emissions over Russia are likely largely underestimated, and their geographical distribution might also be in error. It is therefore possible that these fires were more widespread than in GFED3 and that strong isoprene emission enhancements are not needed to explain the observations.”

5. *Page 12030, Line 1: I find it hard to see that the ratio of 13h30 to 9h30 columns is lower in the model than the satellite for Northern China in Fig. 7, given that the lines are all on top of each other. Can you include values of this ratio somewhere?*

Agreed. The text in Section 7.3 is changed as follows: “This discrepancy is primarily due to the lower modelled ratios of 13h30 to 9h30 columns (average ratio of 1.0 in the model in North China between March and November) compared to the satellite datasets (average ratio of 1.16).”

6. *Page 12031, Line 27: The fluxes attributed to GOME-2 and OMI here are reversed compared to Table 3.*

Corrected.

7. *Section 7.1 and Fig. 15: As the discussion here centers on August 2010, I am assuming that is the month shown in Fig. 15, but the figure caption says March 2010.*

Corrected.

8. *Elimination of passive voice (phrases such as “is found to be” and “is estimated at”) throughout the manuscript would improve flow and more concisely communicate the main points.*

Done.

## Reply to Reviewer#2 comments

The authors would like to thank Reviewer#2 for the positive evaluation of the manuscript, the careful reading and the useful comments and suggestions. Below we address the raised concerns. The reviewer's comments are *italicized*.

*This is an interesting paper that describes the inversion of HCHO columns of GOME-2 (morning orbit) and OMI (afternoon orbit) in the IMAGES model, with the aim to optimise emissions of isoprene, from biomass burning and anthropogenic HCHO sources. Two consistent source of satellite data provide the interesting possibility to study the diurnal behavior, which is done in this paper. The results are interesting, but unfortunately, the paper is rather lengthy with many figures, which does not stimulate (full) reading. The paper provides an interesting contribution, after the following issues have been addressed.*

*Major issues :*

- 1. The structure of the paper is somewhat messy. An example is section 2.2. Here the reader gets very detailed information about anthropogenic VOC emissions and their chemistry without knowing the HCHO budget. This budget should certainly be included in the introduction. I also suggest to move section 2.2 to an Appendix, because it distracts from the main aim of the paper. In the introduction, the authors partly describe their method (e.g. page 12012, 124 and further). Also the paper is a bit short in referencing work of others, and how this study fits in existing knowledge. So, the introduction should be improved in this respect. Further, in section 3.1 reference is made to sensitivity simulations before they have been introduced. It would therefore be good to first do a complete method section, before the discussion of the results. Also, on page 12024, section 5, part of the method is introduced in a section entitled: "Overview of the results". A proper method section would certainly improve the paper. This also gives the opportunity to introduce terms like "ccost function", terms that now pop up without any reference.*

All points suggested by the reviewer have been adopted. More specifically,

- the Subsection 2.2 is moved in the Supplement. Its content is briefly presented in Section 2;
  - a new table is added (Table 1 of the revised version) summarizing all forward sensitivity simulations used to investigate the diurnal variation of HCHO columns. The table is introduced in the first paragraph of Section 3.1;
  - a new section "Inversion methodology" (Section 5) has been added with information on the technique and material from the section "Overview of the results" of the first version of the manuscript;
  - the global budget of HCHO is discussed in the last paragraph of Section 2;
  - more references have been added in the introduction of the revised version.
- 2. The description of the model is slightly misleading. As far as I know, IMAGES uses monthly mean meteorological fields to transport and mix the tracers. This important issue is not clearly mentioned. It would be good to add this, and also add a discussion of its potential impact on the inversion. I expect some impact on the inversion, because of difficulties of co-sampling the model with the observations and potential clear sky biases. Also, in comparing with aircraft*

*observations on page 12027, line 11, there might be issues with monthly-averaged winds, and some words of caution are required.*

The referee is correct that a description of the model transport was lacking. IMAGES uses monthly winds but daily or subdaily fields for other meteorological fields (convection, PBL mixing, temperature, water vapor, rain and cloud fields) and for biogenic isoprene emissions. The model description now includes the following text: “Meteorological fields are obtained from ERA-Interim analyses of the European Centre of Medium-Range Weather Forecasts (ECMWF). Advection is driven by monthly averaged winds, while the effect of wind temporal variability at time scales shorter than one month is represented as horizontal diffusion (Müller and Brasseur, 1995). Convection is parameterized based on daily ERA-Interim updraft mass fluxes. Turbulent mixing in the planetary boundary layer uses daily diffusivities also obtained from ERA-Interim. Rain and cloud fields (and therefore also the photolysis and wet scavenging rates) are also based on daily ERA-Interim fields. The effect of diurnal variations are considered through correction factors on the photolysis and kinetic rates obtained from model simulations accounting for the diurnal cycle of photorates, emissions, convection and boundary layer mixing”.

Regarding the co-sampling of model and observations, the Section 4 now clarifies that “the simulated monthly averaged columns are calculated from daily values weighted by the number of satellite (OMI or GOME-2) measurements for each day at each model grid cell.” Any clear sky bias in the satellite data is therefore taken into account in the model averages.

Finally, the use of monthly winds is not a serious issue in the comparisons of the model with formaldehyde data. Due to the short lifetime of formaldehyde and its precursors (except CH<sub>4</sub> which is well-mixed), long-range transport does not play a significant role, as illustrated by the fact that several recent inverse modelling studies (Palmer et al., 2003; Millet et al., 2008; Barkley et al., 2013) derived isoprene emissions from formaldehyde columns without considering the effects of horizontal transport. To substantiate the weak sensitivity of formaldehyde to the wind fields, the following figure illustrates the impact of 1) halving the wind components in the model (left panel), and 2) using the winds of 2005 instead of 2004 (right panel) on the calculated CH<sub>2</sub>O mixing ratios during INTEX-A. The differences are minor at most locations. The correlation coefficient between the observed and modelled values is decreased from 0.811 in the standard run to 0.806 and 0.809 when using alternative wind sets.

- 3. In the discussion I also would expect some reflection of the separation of biomass burning sources, anthropogenic sources, and isoprene sources. In general, the inversion should give error reductions, and also the posterior co-variance terms that would reflect the ability to separate the different sources. I understand that an error estimate is more difficult for a non-linear system, but the sensitivity experiments give some room for error discussion. But statements on page 12030, line 15: “Chinese isoprene emissions are decreased from 7 Tg year-1 to 6.5 Tg (OMI) and 5.9 Tg (GOME-2)” need to be accompanied by error estimates. I cannot imagine that you can properly separate isoprene HCHO sources from other sources.*

In response to a comment of Reviewer 1, we have now included a discussion of the possible confusion between biomass burning and biogenic emissions over Russia. Over China, biogenic emissions have a distinct seasonal variation and are mostly located in the South, which reduces the possibility of confusion with other categories. We agree however that the separation of posterior emissions between different categories is tentative and subject to errors. However, providing reliable error reductions and posterior co-variances is complex

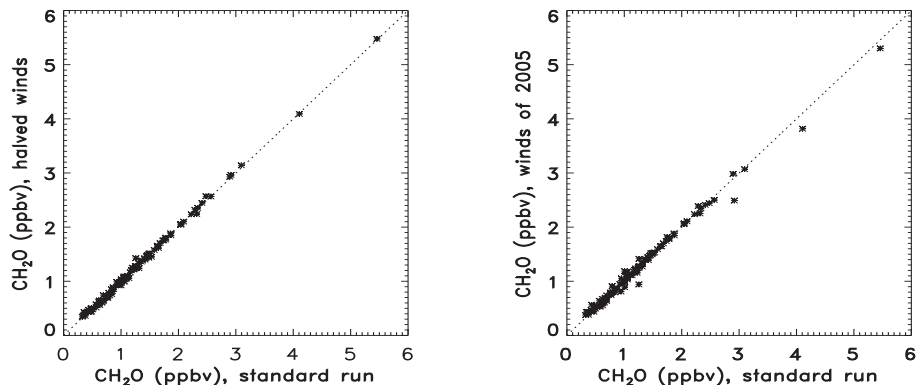


Figure 1: Comparison of the simulated formaldehyde concentrations (average per model gridcell) during the INTEX-A campaign in the standard model run and in a simulation using halved winds (left) and a simulation using the winds of 2005 (right panel).

and somewhat out of scope since the main focus of the present article is a comparison of the inversion results obtained from two sensors. The sensitivity simulations provide indeed some hint regarding the possible uncertainties, and we tried to incorporate their results in the discussion to better reflect the uncertainties.

4. *Units: please check all the units in the paper. They are often missing or incorrect (e.g. TG instead of Tg/year). Also check and add legends to figures. e.g. figure 12: does this show TG/month?*

Units are added where incomplete or missing.

*Minor issues :*

1. *12009, l 23: units are missing*

Units are TgVOC/yr and have been added.

2. *12009, l 25: add per year in the unit*

Done.

3. *12011, l 1: CO and H<sub>2</sub> (add H<sub>2</sub>)*

Added.

4. *12012, l23: The inversion framework is assumed known to the reader. I think it would be could to describe this a bit better in the introduction, i.e. also by referring to earlier studies in this field by other groups.*

The new Section 5 “Inversion methodology” provides some detail about the inversion methodology used to derive top-down VOC emissions. References to earlier studies is provided in the introduction of the revised version.



5. 12013, l2: Here method and introduction are mixed. I would prefer in the introduction references to studies that show the need for these sensitivity studies (e.g. associated with diurnal cycle of emissions). Referring to “inversion design” is a bit too short and methodological.

– The new Table 1 summarizes the sensitivity studies undertaken to investigate the impact of different parameters on the diurnal variation of the HCHO columns. This Table is introduced in the first paragraph of Section 3.

– The sentence now reads : “Sensitivity studies are carried out to assess the robustness of the findings to different assumptions, e.g. to changes of the prescribed a priori errors on the emission fluxes in the inversion.”

6. 12014: l7: add unit kg/kmol (or g/mol)

Units added.

7. 12014: l14: “The African. . .worldwide”. Maybe good to add some cautious remarks here. Over peat fires (e.g. Russia in section 6.2) this assumption is certainly not valid, and maybe also not for boreal fires.

The sentence now reads : “This profile is in fairly good agreement with the averaged diurnal cycle of active fire observations constructed from the GOES geostationary satellite encompassing North, Central and South America (Mu et al. 2011), and therefore it is applied to all fires worldwide. Note, however, that this specific temporal profile might not be appropriate for some locations, e.g. peat fires over Russia.”

8. 12015, l9: I miss somehow some recent references, e.g. Fuchs, H. et al. *Experimental evidence for efficient hydroxyl radical regeneration in isoprene oxidation. Nature Geosci.* 6, 102320131026 (2013).

Reference added.

9. 12017, l3: I would use something like (g CHCO/g OAHC) as unit here.

Replaced, cf. Supplementary material.

10. 12018, l10 (and further on): on Fig. xx → in Fig. xx

Corrected.

11. 12020, l14: please repeat that you evaluate the diurnal cycle in the column, and not in the near surface concentration.

The sentence now reads : “To evaluate the diurnal cycle of the modelled HCHO column...”

12. 12022, l3: here I wonder why the modeled HCHO concentrations in the boundary layer are not compared to observations. I agree that boundary layer mixing complicates issues here, but the authors should at least argue why they did not evaluate the model with other HCHO measurements. Also, by comparing only diurnal profiles they might hide deficiencies in the model.

We now provide in the Introduction a more clear argument for using ground-based column measurements instead of in situ concentration measurements: “Field campaign measurements show that the diurnal patterns of surface HCHO concentrations are mostly influenced by

the magnitude and diurnal variability of precursor emissions and the development of the boundary layer. (...) Long-term diurnal measurements of HCHO columns are limited, but are less influenced by variations in boundary layer mixing and are directly comparable with the satellite observations.”

13. 12023, l29: *on this figure → in this figure*

Corrected.

14. 12024, l16: *Table 2 lists other sensitivity studies than described earlier in the discussion of the diurnal profiles. I suggest to include one table with all simulations performed.*

A new Table is added summarizing all forward tests performed to investigate the diurnal cycle of HCHO columns. Section 3 and the caption of Figure 2 make reference to this Table.

15. 12031, l8, *acronym IASI is introduced, but was used before*

The acronym is now mentioned in the introduction.

16. 12033, l3: *contrasted → contrasting*

Corrected.

17. 12033, l14: *Tropical Asia emissions have been studied using IASI: (Basu, S. et al. The seasonal variation of the CO<sub>2</sub> flux over Tropical Asia estimated from GOSAT, CONTRAIL, and IASI. Geophys Res Lett 41, 1809–1815 (2014))*

Agreed. We modified the discussion of the IASI CO results over Indochina (Section 8.3) as follows: “Indeed, as seen on the lower panel of Fig. 14, modelled CO simulations using biomass burning fluxes optimized using OMI data (i.e. reduced by ca. 26% in March relative to GFED3) display a better agreement with the observed CO columns, despite an underestimation by ~10% over most of the peninsula. This result is consistent with the moderate reduction (ca. 20% in March) of biomass burning emissions of CO over Tropical Asia inferred by Basu et al. (2014) in an inversion based on IASI CO columns utilizing the TM5 atmospheric model with GFED3 as a priori inventory. ”

18. 12035, l27: *and (to a lesser extent) meteorological parameters. It is unclear what is meant with this statement.*

The influence of the diurnal cycle of meteorological parameters on the diurnal cycle of HCHO columns is expected to be minor, as confirmed by sensitivity simulations (with diurnally constant convection and PBL mixing). Photochemistry and the emissions are the main players. The influence of meteorological parameters is mentioned here for completeness.

19. *Figure 2: Please use a common y-axis metric.*

Done.

20. *Figure 9: the order of the panels does not make sense. Jan-mar-aug-oct? why not Jan, Apr, Jul, Oct?*

March and August coincide with the fire peak season in Indochina and Amazonia, respectively. Because these regions are discussed in detail in our manuscript, we believe that including these two months (instead of April and July) in Figure 9 makes more sense and facilitates the discussion.

## How consistent are top-down hydrocarbon emissions based on formaldehyde observations from GOME-2 and OMI?

T. Stavrou<sup>1</sup>, J.-F. Müller<sup>1</sup>, M. Bauwens<sup>1</sup>, I. De Smedt<sup>1</sup>, M. Van Roozendael<sup>1</sup>, M. De Mazière<sup>1</sup>, C. Vigouroux<sup>1</sup>, F. Hendrick<sup>1</sup>, M. George<sup>2</sup>, C. Clerbaux<sup>2,3</sup>, P.-F. Coheur<sup>3</sup>, and A. Guenther<sup>4</sup>

<sup>1</sup>Belgian Institute for Space Aeronomy, Avenue Circulaire 3, 1180, Brussels, Belgium

<sup>2</sup>UPMC Univ. Paris 6; Université Versailles St.-Quentin; CNRS/INSU, LATMOS-IPSL, 75252, Cedex 05, Paris, France

<sup>3</sup>Spectroscopie de l'Atmosphère, Service de Chimie Quantique et Photophysique, Université Libre de Bruxelles, 1050, Belgium

<sup>4</sup>Atmospheric Sciences and Global Change Division, Pacific Northwest National Laboratory, Richland, Washington State, USA

### Abstract.

The vertical columns of formaldehyde (HCHO) retrieved from two satellite instruments, the Global Ozone Monitoring Instrument-2 (GOME-2) on Metop-A and the Ozone Monitoring Instrument (OMI) on Aura, are used to constrain global emissions of HCHO precursors from open fires, vegetation and human activities in the year 2010. To this end, the emissions are varied and optimized using the adjoint model technique in the IMAGESv2 global CTM (chemistry-transport model) on a monthly basis and at the model resolution. Given the different local overpass times of GOME-2 (9h30) and OMI (13h30), the simulated diurnal cycle of HCHO columns is investigated and evaluated against ground-based optical measurements at 7 sites in Europe, China and Africa. The modelled diurnal cycle exhibits large variability, reflecting competition between photochemistry and emission variations, with noon or early afternoon maxima at remote locations (oceans) and in regions dominated by anthropogenic emissions, late afternoon or evening maxima over fire scenes, and midday minima in isoprene-rich regions. The agreement between simulated and ground-based columns is ~~found to be~~ generally better in summer (with a clear afternoon maximum at mid-latitude sites) than in winter, and the annually averaged ratio of afternoon to morning columns is slightly higher in the model (1.126) than in the ground-based measurements (1.043).

The anthropogenic VOC (volatile organic compound)

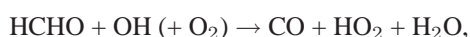
sources are found to be weakly constrained by the inversions on the global scale, mainly owing to their generally minor contribution to the HCHO columns, except over strongly polluted regions, like China. The OMI-based inversion yields total flux estimates over China close to the bottom-up inventory (24.6 vs. 25.5 TgVOC/yr in the a priori) with, however, pronounced increases in the Northeast China and reductions in the south. Lower fluxes are estimated based on GOME-2 HCHO columns (20.6 TgVOC/yr), in particular over the Northeast, likely reflecting mismatches between the observed and the modelled diurnal cycle in this region.

The resulting biogenic and pyrogenic flux estimates from both optimizations generally show a good degree of consistency. A reduction of the global annual biogenic emissions of isoprene is derived, by 9% and by 13% according to GOME-2 and OMI, respectively, compared to the a priori estimate of 363 Tg in 2010. The reduction is largest (up to 25-40%) in the Southeastern US, in accordance with earlier studies. The GOME-2 and OMI satellite columns suggest a global pyrogenic flux decrease by 36% and 33%, respectively, compared to the GFEDv3 inventory. This decrease is especially pronounced over tropical forests such as Amazonia and Thailand/Myanmar, and is supported by comparisons with ~~IASI CO observations~~ [CO observations from IASI \(Infrared Atmospheric Sounding Interferometer\)](#). In contrast to these flux reductions, the emissions due to harvest waste burning are strongly enhanced in the Northeastern China plain in June (by ca. 70% in June according to

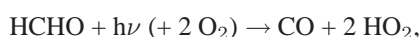
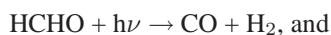
OMI) as well as over Indochina in March. Sensitivity inversions showed robustness of the inferred estimates, which were found to lie within 7% of the standard inversion results at the global scale.

## 1 Introduction

Besides a small direct source, the dominant source of formaldehyde (HCHO) is its photochemical formation due to the oxidation of methane and non-methane volatile organic compounds (NMVOCs) emitted by the biosphere, vegetation fires and human activities. Methane oxidation is by far the largest contributor to the HCHO formation (ca. 60% on the global scale), while the remainder is due to oxidation of a large variety of VOCs of anthropogenic, pyrogenic and biogenic origin (Stavrakou et al., 2009a). The main removal processes (Sander et al., 2011) are the oxidation by OH,



ultimately producing CO and converting OH to HO<sub>2</sub>, and photolysis reactions



producing CO, H<sub>2</sub> as well as HO<sub>2</sub> radicals.

Because of its short photochemical lifetime (ca. 4–5 hours), and of the short lifetime of its main NMVOC precursors, most importantly isoprene, enhanced levels of HCHO are directly associated with the presence of nearby hydrocarbon emission sources. ~~The strong potential of HCHO measurement to constrain VOC emission fluxes on global and regional scales was put forward. Relying on the measurement of HCHO column densities from space by solar backscatter radiation in the UV-Visible spectral region~~

(Chance et al., 2000; De Smedt et al., 2008, 2012; Hewson et al., 2013; De Smedt et al., 2015; González Abad et al., 2015), ~~the use of HCHO measurements to inform about the VOC precursor fluxes was explored~~ through a large body of literature studies, ~~relying on the measurement of HCHO column densities from space by solar backscatter radiation in the UV-Visible spectral region. In some cases, however, these studies led to conflicting answers.~~

~~The first studies focused on the derivation of isoprene fluxes in the U.S. constrained by HCHO columns from~~

~~GOME or OMI instruments (Palmer et al., 2003, 2006; Millet et al., 2006, 2008). The estimation of isoprene emissions was extended to cover other regions, e.g. South America (Barkley et al., 2008, 2009) and Africa (Marais et al., 2012, 2014), with special efforts to exclude satellite scenes affected by biomass burning, and Europe (Dufour et al., 2009). Fu et al. (2007) reported top-down isoprene and anthropogenic reactive VOCs fluxes over East and South Asia, and more recently anthropogenic emissions of reactive VOCs in eastern Texas were estimated using the oversampling technique applied to OMI HCHO observations (Zhu et al., 2015). Based on SCIAMACHY observations, space-based emissions of isoprene and pyrogenic NMVOCs were derived on the global scale using the adjoint model approach (Stavrakou et al., 2009b,c). Each of those studies was constrained by one satellite dataset, and in many cases, conflicting answers were found regarding the magnitude and/or spatiotemporal variability of the underlying VOC sources, mostly owing to differences in the satellite column products, in the models used to infer top-down estimates through inversion techniques, and in the emission inventories used as input in the models. The latter point is very often a source of confusion, since a very large range of estimates can be obtained using the same emission model depending on the choice of input variables. Indeed, the isoprene fluxes estimated using MEGAN (Guenther et al., 2006), the most commonly used bottom-up emission model for biospheric emissions, are found to strongly vary vary strongly depending on the driving variables used (e.g. meteorology, landcover), leading to an uncertainty of about a factor of 5 for the global isoprene emissions (Arneth et al., 2011) and underscoring the need for clearly indicated a priori emission information in order to allow meaningful comparisons between inverse modelling different studies.~~

~~Despite significant progress in the field, the derivation of VOC emissions using HCHO columns remains challenging, mainly owing to the large number and diversity of HCHO precursors, to uncertainties regarding their sources and speciation profiles, and to inadequate or incomplete knowledge of their chemical mechanisms and pathways leading to HCHO formation. In addition, it crucially depends on the quality of the satellite retrievals, and therefore efforts to address as-~~

~~GOME or OMI instruments (Palmer et al., 2003, 2006; Millet et al., 2006, 2008). The estimation of isoprene emissions was extended to cover other regions, e.g. South America (Barkley et al., 2008, 2009) and Africa (Marais et al., 2012, 2014), with special efforts to exclude satellite scenes affected by biomass burning, and Europe (Dufour et al., 2009). Fu et al. (2007) reported top-down isoprene and anthropogenic reactive VOCs fluxes over East and South Asia, and more recently anthropogenic emissions of reactive VOCs in eastern Texas were estimated using the oversampling technique applied to OMI HCHO observations (Zhu et al., 2015). Based on SCIAMACHY observations, space-based emissions of isoprene and pyrogenic NMVOCs were derived on the global scale using the adjoint model approach (Stavrakou et al., 2009b,c). Each of those studies was constrained by one satellite dataset, and in many cases, conflicting answers were found regarding the magnitude and/or spatiotemporal variability of the underlying VOC sources, mostly owing to differences in the satellite column products, in the models used to infer top-down estimates through inversion techniques, and in the emission inventories used as input in the models. The latter point is very often a source of confusion, since a very large range of estimates can be obtained using the same emission model depending on the choice of input variables. Indeed, the isoprene fluxes estimated using MEGAN (Guenther et al., 2006), the most commonly used bottom-up emission model for biospheric emissions, are found to strongly vary vary strongly depending on the driving variables used (e.g. meteorology, landcover), leading to an uncertainty of about a factor of 5 for the global isoprene emissions (Arneth et al., 2011) and underscoring the need for clearly indicated a priori emission information in order to allow meaningful comparisons between inverse modelling different studies.~~

Despite significant progress in the field, the derivation of VOC emissions using HCHO columns remains challenging, mainly owing to the large number and diversity of HCHO precursors, to uncertainties regarding their sources and speciation profiles, and to inadequate or incomplete knowledge of their chemical mechanisms and pathways leading to HCHO formation. In addition, it crucially depends on the quality of the satellite retrievals, and therefore efforts to address as-

pects such as instrumental degradation, temporal stability of the retrievals, noise reduction, and error characterization are of primary importance (De Smedt et al., 2012, 2015; Hewson et al., 2013; González Abad et al., 2015).

The diurnal cycle of HCHO concentrations has been investigated in field studies in different environments. At a tropical forest location in Borneo, a advent of new satellites measuring at different overpass times, like GOME-2, SCIAMACHY and OMI, opens new avenues in the derivation of top-down estimates. However, it also raises new questions regarding the consistency of the estimated fluxes from different instruments. Indeed, a recent study focusing on Tropical South America reported a factor of 2 difference between the SCIAMACHY- and OMI-based isoprene fluxes derived using the same model, a difference which apparently could not be explained by differences in the sampling features of the sensors or by uncertainties in the air mass factor calculations, and which might be partly due to model deficiencies pertaining to the diurnal cycle of the HCHO columns (Barkley et al., 2013)

The main objective of this study is therefore to address the issue of consistency between global VOC flux strengths inferred from one complete year of GOME-2 and OMI HCHO column densities, taking into account their different overpass times. Field campaign measurements show that the diurnal patterns of surface HCHO concentrations are mostly influenced by the magnitude and diurnal variability of precursor emissions and the development of the boundary layer. A midday peak followed by gradual decrease in the evening were observed. At a forest site in California, HCHO concentration was observed to peak concentrations were observed at a tropical forest in Borneo (MacDonald et al., 2012), whereas HCHO concentration peaked in the evening during cool days and around midday under in warm and sunny conditions at a forest site in California (Choi et al., 2010). Similar diel patterns were observed and near a city location in the Po valley (Junker-mann, 2009). Generally, the diurnal patterns of surface HCHO concentrations are found to be mostly influenced by the magnitude of precursor emissions and their diurnal variability, as well as the development of the boundary layer. Diurnal measurements of HCHO columns are unfortunately

~~more limited. Measurements over the remote ocean using the MAX-DOAS technique showed noontime maxima and low morning and evening values. The observation of HCHO columns by GOME-2 and OMI at different times (9h30 and 13h30) offer a potentially useful additional piece of information in this respect.~~

Our first objective is to investigate Long-term diurnal measurements of HCHO columns are limited, but are less influenced by variations in boundary layer mixing and are directly comparable with the satellite observations. Here, we investigate first the diurnal variability of HCHO columns simulated by the IMAGESv2 global CTM, and in particular, to evaluate the model capability skill to reproduce the observed diurnal cycle of HCHO columns at different locations. The main focus of this study is to address the issue of consistency between VOC flux strengths inferred from one complete year of

Retrieved HCHO columns from GOME-2 and OMI HCHO column densities, taking into account their different instrument overpass times. For that purpose, the satellite, with local overpass times 9h30 and 13h30, respectively, are used to constrain the VOC emissions. The algorithms developed for the two sensors were designed to ensure the maximum consistency between the two sets of observations. The inversion framework uses the adjoint model, as described in detail in De Smedt et al. (2015). The top-down emission estimates are derived using an inversion framework based on the adjoint of the IMAGESv2 CTM (Müller and Stavrakou, 2005; Stavrakou et al., 2009a) and fluxes are optimized per month, model grid and emission category (anthropogenic, biogenic and pyrogenic). The same inversion setup is applied using either GOME-2 or OMI measurements as top-down constraints for 2010, a particularly warm and dry year with intense fires and enhanced biogenic emissions. Sensitivity studies are carried out to assess the robustness of the findings to different assumptions, e.g. to the inversion design changes of the prescribed a priori errors on the emission fluxes in the inversion.

In Sect. 2 a brief description of the IMAGESv2 model is given, with particular focus on briefly described and the HCHO budget is discussed, whereas the formation of HCHO in the oxidation of anthropogenic VOCs (Sect. ??) is

[presented in detail in the Supplement](#). The modelled and observed diurnal cycle of HCHO columns is discussed in [detail in Sect. 3](#). The ~~GOME-2 and OMI HCHO columns are briefly discussed~~ [satellite HCHO columns used to constrain the inversions and the inversion methodology are presented in Sect. 4 and 5](#). An overview of the ~~emissions results~~ [inferred from the inversions using GOME-2 and OMI data as well as and](#) global results from sensitivity case studies are presented in Sect. 6. The VOC emissions inferred at the mid-latitudes (North America, China) and in tropical regions (Amazonia, Indonesia, Indochina, Africa) are thoroughly described in Sect. 7 and 8. Finally, conclusions are drawn in Sect. 9.

## 2 HCHO simulated with IMAGESv2

### 2.1 Brief model description

The IMAGESv2 global CTM is run at  $2^\circ \times 2.5^\circ$  horizontal resolution and extends vertically from the Earth's surface to the lower stratosphere through 40 unevenly spaced sigma-pressure levels. It calculates daily averaged concentrations of 131 transported and 41 short-lived trace gases with a time step of 6 hours. [Meteorological fields are obtained from ERA-Interim analyses of the European Centre of Medium-Range Weather Forecasts \(ECMWF\). Advection is driven by monthly averaged winds, while the effect of wind temporal variability at time scales shorter than one month is represented as horizontal diffusion](#) (Müller and Brousseau, 1995). [Convection is parameterized based on daily ERA-Interim updraft mass fluxes. Turbulent mixing in the planetary boundary layer uses daily diffusivities also obtained from ERA-Interim. Rain and cloud fields \(and therefore also the photolysis and wet scavenging rates\) are also based on daily ERA-Interim fields.](#) The effect of diurnal variations are considered through correction factors on the photolysis and kinetic rates obtained from model simulations accounting for the diurnal cycle of photolysis, emissions ~~and meteorological variables~~, [convection and boundary layer mixing](#) (Stavrakou et al., 2009a). A thorough model description is given in Stavrakou et al. (2013) and references therein. The target year of this study is 2010.

Anthropogenic emissions are obtained from the RETRO 2000 database (<http://retro.enes.org>, Schultz et al. (2008)), except over Asia where the REASv2 inventory for year 2008 is used (Kurokawa et al., 2013). The diurnal profile of anthropogenic emissions follows Jenkin et al. (2000). Isoprene emissions (including their diurnal, day-to-day and seasonal variations) are obtained from the MEGAN-MOHYCAN-v2 inventory (<http://tropo.aeronomie.be/models/isoprene.htm>, Müller et al. (2008); Stavrakou et al. (2014)) and are estimated at 363 Tg in 2010 (Fig. ??). [Monthly averaged biogenic methanol emissions \(~100 Tg/year globally\) are taken from a previous inverse modelling study](#) (Stavrakou et al., 2011) [using IMAGESv2 and methanol total columns from IASI. Biogenic emissions of acetaldehyde \(22 Tg/year\) and ethanol \(22 Tg/year\) are calculated following](#) Millet et al. (2010)

Open vegetation fire emissions are taken from GFEDv3 (van der Werf et al., 2010), with emission factors for tropical, extratropical, savanna and peat fire burning provided from the 2011 update of the recommendations by Andreae and Merlet (2001). The GFEDv3 emission is estimated at 105.4 TgVOC in 2010, equivalent to 2.26 Tmoles (average molecular weight of 46.5 kg/kmol) (Fig. ??). The diurnal profile of biomass burning emissions was derived based on a complete year of geostationary active fires and fire radiative power observations from the SEVIRI imager over Africa (Roberts et al., 2009). The analysis of the fire cycle, performed over 20 different land cover types in the Northern and Southern Hemisphere Africa, exhibits strong diurnal variability and very similar patterns in both hemispheres. According to this dataset, fire activity is negligible during the night and low in the early morning, it peaks around 13h30 local time, and decreases rapidly in the afternoon hours. ~~The African diurnal profile has been~~ [This profile is in fairly good agreement with the averaged diurnal cycle of active fire observations constructed from the GOES geostationary satellite encompassing North, Central and South America](#) (Mu et al., 2011), [and therefore it is applied to all fires worldwide.](#)

The vertical profiles of pyrogenic emissions are taken from a new global dataset (Sofiev et al., 2013) of vertical smoke profiles from open fires, based on plume top heights com-

puted by a semi-empirical model (Sofiev et al., 2012), and  
 305 fire radiative power from the MODIS instrument. These pro-  
 files are highly variable depending on the season and the year.  
 Forest regions are characterized by high altitude plumes (up  
 to 6-8 km), whereas grasslands generally emit within 2-3 km.  
 About half of emitted flux is injected within the boundary  
 310 layer. The 5<sup>th</sup>, median, 80<sup>th</sup> and 99<sup>th</sup> monthly percentiles  
 of injection profiles maps of this dataset were obtained from  
 the GlobEmission website (<http://www.globemission.eu>) and  
 implemented in the CTM.

The chemical mechanism of isoprene oxidation accounts  
 315 for OH recycling according to the Leuven Isoprene mech-  
 anism LIM0 (Peeters et al. (2009); Peeters and Müller  
 (2010); Stavrakou et al. (2010)), and its upgraded ver-  
 sion LIM1 (Peeters et al., 2014). LIM1 is based on a  
 theoretical re-evaluation of the kinetics of isoprene per-  
 320 oxy radicals undergoing 1,5 and 1,6-shift isomerization,  
 and is ~~found to be~~ in satisfactory agreement (factor of  
 ~2) with experimental yields of the hydroperoxy aldehy-  
 des (HPALDs) believed to be major isomerization products  
 (Crouse et al., 2011). Based on box model calculations  
 325 using the ~~KineticPreProcessor~~ Kinetic PreProcessor (KPP)  
 chemical solver (Damian et al., 2002), the isomerization of  
 isoprene peroxy radicals is estimated to decrease the molar  
 HCHO yield by ~8% in high NO<sub>x</sub> conditions (2.39 vs. 2.60  
 mol/mol after two months of simulation at 1 ppbv NO<sub>2</sub>),  
 330 and by ~15% in low NO<sub>x</sub> conditions (1.91 vs. 2.25 after  
 two months at 0.1 ppbv NO<sub>2</sub>). These estimated changes are  
 however very uncertain, given their dependence on the uni-  
 molecular reaction rates of isoprene peroxy radicals and on  
 the poorly constrained fate of the isomerization products. 375

## 2.1 HCHO from anthropogenic NMVOC emissions

~~Based on the NMVOC speciation profile of~~ The speciation  
profile for anthropogenic NMVOC emissions is based on  
 the UK National Atmospheric Emissions Inventory (NAEI)  
 340 (Goodwin et al. (2001)). According to NAEI, 49 (out  
 of the 650 considered) compounds account for ca. 81%  
 of the total UK emission. ~~17 of the 49 compounds are~~  
~~included explicitly out of them are explicitly accounted for~~  
 in IMAGESv2, ~~namely, ethane, propane, ethene, propene,~~  
~~acetylene, formaldehyde, acetaldehyde, propanal, benzene,~~

~~toluene, xylenes, methanol, ethanol, formic acid, acetic~~  
~~acid, acetone, and methyl ethyl ketone. The remaining~~  
~~32 species (Table ??) are taken into account through~~ while  
 a lumped compound, ~~OAHC~~ (other anthropogenic hydro-  
 carbons) ~~. The oxidation accounts for the remaining 32~~  
~~species. The chemical~~ mechanism of OAHC is ~~adjusted~~  
~~adapted~~ in order to reproduce the yields of HCHO from  
 the mix of 32 higher NMVOCs. This ~~adjustment~~ is real-  
 ized based on time-dependent box model calculations using  
 the semi-explicit Master Chemical Mechanism (MCMv3.2,  
<http://mcm.leeds.ac.uk/MCM/>, Saunders et al. (2003); Bloss  
 et al. (2005)).

~~The NO<sub>2</sub> concentration is kept equal to~~ Based on  
IMAGESv2 model simulations, the global annual HCHO  
budget is estimated at 1600 Tg HCHO and is dominated  
~~by photochemical production, whereas less than 1 ppb since~~  
~~our focus is on environments dominated by anthropogenic~~  
~~activities. For each NMVOC, the % is due to direct~~  
~~emissions. The most important source of HCHO yield is~~  
~~calculated after one day of simulation (short term) and after~~  
~~is methane oxidation~~ (60

~~The calculated short term and final molar yields are~~  
~~summarized in Table ??.~~ As expected, the highest short term  
~~yields are calculated for the most reactive precursors,~~  
~~namely, the higher alkenes and aromatics, with  $k_{OH}$  typically~~  
~~ranging between  $3 \cdot 10^{-11}$  and  $7 \cdot 10^{-11} \text{ cm}^3 \text{ molec.}^{-1} \text{ s}^{-1}$ .~~  
~~For those compounds, the short term yield and the final~~  
~~yield are very close, within ~10%.~~ Exceptions are  
~~the cases of ethylbenzene, which is less reactive, and~~  
~~2-methylpropene, which is oxidized to acetone, a very~~  
~~slow reacting intermediate. For alkanes, alcohols and esters,~~  
~~the short term yield is often much lower than the final yield,~~  
~~globally, the remainder being~~ due to the

~~The production of HCHO (in g) by a NMVOC can be~~  
~~expressed as~~

$$P = E \cdot Y \cdot MW_{\text{HCHO}} / MW_{\text{NMVOC}},$$

~~with  $E$  the emission (in g) oxidation of biogenic (30%),  $Y$~~   
~~the calculated short term or final molar yield and  $MW$  the~~  
~~molecular weight.~~

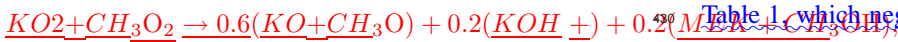
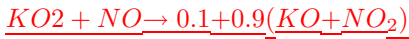
$$MW_{\text{OAHC}} = \frac{\sum_i E_i}{\sum_i (E_i / MW_i)},$$

and its short term and final yield by

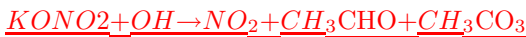
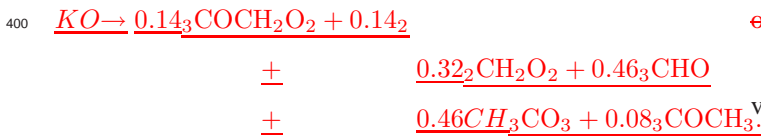
$$Y_{\text{OAHC}} = \frac{\sum_i (E_i / \text{MW}_i) \cdot Y_i}{\sum_i E_i / \text{MW}_i}$$

The values obtained in this way are 73 g/mol for  $\text{MW}_{\text{OAHC}}$  anthropogenic (7%) and 0.567 pyrogenic (3%) hydrocarbons (Stavrakou et al., 2009a). The main removal process is photolysis, which accounts for 70% of the global sink, followed by OH oxidation (26%), and

The rate of the reaction of OAHC with OH,



where MEK denotes methylethyl ketone, KOH is a generic higher alcohol and the oxy radical (KO) reacts immediately following



where BIACET denotes biacetyl ( $\text{CH}_3\text{COCOCH}_3$ ). The kinetic rates are  $k_{\text{KO}} = 2.54 \cdot 10^{-12} \exp(360/T)$ ,  $k_{\text{KO}_2} = 1.82 \cdot 10^{-13} \exp(1300/T)$ ,  $k_{\text{KO}_2 + \text{NO}} = 3.8 \cdot 10^{-13}$ ,  $k_{\text{KO}_2 + \text{HO}_2} = 10^{-12}$ , and  $k_{\text{KO}_2 + \text{CH}_3\text{O}_2} = 3.9 \cdot 10^{-11}$  (in  $\text{cm}^3 \text{molec.}^{-1} \text{s}^{-1}$ ), where  $T$  denotes the temperature by dry and wet deposition. The aforementioned production and loss processes result in a global lifetime of 4.6 hours.

### 3 Diurnal cycle of HCHO columns

#### 3.1 Model processes and sensitivity

The top-down determination of VOC emissions based on GOME-2 and OMI data assumes that the model reproduces reasonably well the diurnal cycle of HCHO columns. To test this assumption would require a large number of well distributed ground-based observations, which are however scarce and intermittent. We present further below a comparison with a limited dataset of column observations at surface sites, most of which are located at or near pollution centers at mid-latitudes. In order to better characterize the diurnal cycle and to identify the factors influencing it in the model, we present in Fig. ?? the modelled diurnal variations of HCHO columns at selected locations, and in Fig. ?? the distribution of the local time of the maximum in the diurnal cycle of HCHO columns. Fig. ?? also shows displays the results of sensitivity calculations either neglecting described in Table 1, which neglect either the diurnal cycle of emissions (in blue) or neglecting NDC) or the biomass burning emissions (in orange NBB), in comparison to the standard model results (in red). Several. The results of additional sensitivity simulations were conducted, the results are however related to vertical transport (Table 1) are not shown here for the sake of clarity.

A striking feature of Fig. ?? and Fig. ?? is the large diversity of diurnal profiles across the seasons and locations. Very little HCHO variations are seen at high latitudes during the winter, due to the very low photochemical activity and absence of notable emissions. In regions where anthropogenic emissions are the dominant source of HCHO precursors, such as Northwestern Europe, Eastern China, India and the Middle East (Fig. ??), the diurnal cycle displays a midday maximum and a minimum at the end of the night (Fig. ??, S. England and Fig. ??). As can be seen in Fig. ??, the diurnal cycle of anthropogenic emissions has a very small impact at these locations. This is due to the fairly long photochemical lifetimes of most anthropogenic NMVOCs. Their relatively low short-term HCHO yields in comparison with the final yields (see Table 1) implies that most HCHO formation occurs days after the precursor has been emitted. The midday maximum therefore reflects the diurnal cycle of OH concen-



trations, very low at night and maximum when radiation is highest (Logan et al., 1981).

Over the Eastern US, the wintertime (November to March) diurnal cycle displays a similar pattern due to anthropogenic emissions. In the summer, however, when biogenic isoprene is the dominant VOC, a completely different behavior is predicted, with a noon minimum and a maximum in the evening or even in the early morning (Fig. ??, Arkansas and Fig. ??). A relatively similar pattern is found in the Manaus region in the Amazon in July-September (Fig. ??), in agreement with a previous modelling study using GEOS-Chem and focussing on Amazonia (Barkley et al., 2011). At all sites impacted by isoprene (Arkansas, Borneo, Manaus and Mato Grosso), the simulation neglecting diurnal variations of emissions (Fig. ??, [NDC](#), blue curve) leads to a continuous HCHO buildup during the night and to a pronounced morning maximum followed by a gradual decrease during daytime until a minimum in late afternoon or early evening. The nighttime buildup in that simulation follows the slow isoprene oxidation (mostly by ozone) and the near-absence of HCHO sinks, whereas the gradual HCHO decrease during the day reflects the decline of the accumulated isoprene and intermediate oxidation products due to OH oxidation. Although the daytime chemical lifetime of isoprene is short (less than 1 hour at an OH concentration of  $4 \cdot 10^6 \text{ molec.cm}^{-3}$ ), a large fraction of the formaldehyde production due to isoprene involves longer-lived intermediates (such as methylvinylketone, methacrolein, hydroxyacetone, hydroperoxides, etc.) resulting in a delayed formaldehyde production.

When the diurnal cycle of isoprene emissions is taken into account (Fig. ??, [STD](#), red curve), the midday emission maximum leads to a HCHO minimum and to an increase afterwards, due to the delayed production from isoprene (Arkansas, Manaus and Mato Grosso). It has been pointed out (Barkley et al., 2011) that the nighttime HCHO accumulation and morning maximum near Manaus in September might be unrealistic, as models are often unable to reproduce the observed rapid decline of isoprene concentrations during the evening at different surface sites. Nighttime chemistry, deposition and boundary layer processes might indeed be poorly represented in models, causing significant deviations

from the patterns described above. As is obvious from Figs. ?? and ??, different locations or seasons display often very different diurnal patterns, for complex reasons including radiation and NO<sub>x</sub> levels, the occurrence of biomass burning, mixing processes, etc. Note however, that sensitivity simulations neglecting the diurnal cycle of boundary layer mixing and deep convection fluxes were found to cause only minimal deviations from the columns of the standard model calculations.

Vegetation fires are found to cause locally very strong variations with maximum values in the evening, exceeding by up to 70% the morning minimum value (Central Alaska in May and July, Mato Grosso in September). As seen ~~on~~ [in](#) Fig. ??, strong emissions over Eastern Siberia, European Russia, Central Canada, Angola, Brazil and Northern Australia are most often associated with HCHO column maxima in the late afternoon and evening.

### 3.2 Model evaluation

To evaluate the ~~model diurnal cycle~~ [diurnal cycle of the modelled HCHO column](#), we use ground-based remote-sensed measurements at the 7 following sites :

1. Cabauw/The Netherlands (52°N, 5° E), 8 June – 21 July 2009 (Pinaridi et al., 2013)
2. Observatoire de Haute Provence (OHP)/France (43.94°N, 5.71°E), 26 June 2007 – 20 March 2013 (Valks et al., 2011)
3. Uccle/Belgium (50.78°N, 4.35°E), 1 May 2011 – 23 April 2012 (Gielen et al., 2014)
4. Beijing/China (39.98°N, 116.38°E), 3 July 2008 – 17 April 2009 (Vlemmix et al. (2015), see also Hendrick et al. (2014))
5. Xianghe/China (39.75°N, 116.96°E), 7 March 2010 – 26 December 2013 (Vlemmix et al. (2015), see also Hendrick et al. (2014))
6. Bujumbura/Burundi (3°S, 29°E), 25 November 2013 – 22 January 2014 (De Smedt et al., 2015)
7. Reunion Island/France (20.9°S, 55.5°E), 1 August 2004 – 25 October 2004, 21 May 2007 – 15 October 2007, 2

June 2009 – 28 December 2009, and 11 January 2010 –  
16 December 2010 (Vigouroux et al., 2009).

The MAX-DOAS (Multi-axis differential optical absorption spectroscopy) technique (Hönninger et al., 2004; Platt and Stutz, 2008) was used in all cases, except at Reunion Island where the FTIR (Fourier Transform infrared spectroscopy) technique is used (Griffiths and de Haseth, 2007; Vigouroux et al., 2009). Total HCHO columns are measured at all stations, and profiles are also measured at Beijing, Xianghe, and Bujumbura.

Figures ?? and ?? illustrate the diurnal cycle of observed and modelled HCHO columns seasonally averaged and normalized by their noon values. The ratio of the observed columns at 13h30 and 9h30 ranges mostly between 0.8 and 1.2, although values close to 1.4 are found at one site (OHP). The modelled values of this ratio are most often higher than in the measurements, except at OHP. The average ratio at all sites and seasons is slightly higher in the model (1.126) than in the data (1.043), although the average absolute deviation between model and data is large (20%), presumably mostly because of representativity issues. The coarse resolution of the model makes it impossible to reproduce the very large differences seen, for example, between the observed diurnal profiles at Beijing and Xianghe, two very nearby sites lying in the same model grid cell. OHP similarly lies in a region with strong gradients in the diurnal behavior of the columns, as seen in Fig. ??.

Nevertheless, the diurnal cycle of HCHO columns at the four most polluted sites (Uccle, Cabauw, Beijing and Xianghe) shows a consistent pattern during summertime (also in spring and fall at Uccle) which is well reproduced by the model. At Reunion Island as well, the observed midday maximum is well reproduced by the model. As pointed out above, the midday maximum at both very remote and very polluted sites is primarily caused by the diurnal cycle of OH levels, as the reaction with OH of the (mostly fairly long-lived) anthropogenic VOCs as well as methane is the main source of HCHO in those areas. In the Beijing area, the diurnal cycle of emissions is responsible for a slight delay in the maximum towards the afternoon, in agreement with the observations.

A broader network of measurements would be necessary to provide a more detailed assessment of HCHO column diurnal variations, in particular over forests and in biomass burning areas. Nevertheless, the comparison presented above with the limited dataset of available measurements revealed no large systematic discrepancies, except for a slight overestimation (by 8%) of the average ratio of 13h30 to 9h30 columns.

#### 4 Satellite observations

The current version (v14) of the HCHO retrievals applied to GOME-2/METOP-A and OMI/AURA measurements is based on the algorithm developed for GOME-2 (version 12, De Smedt et al. (2012)), but with significant adaptations, as detailed below.

A classical DOAS algorithm is used, including three main steps: (1) the fit of absorption cross-section databases to the measured Earth reflectance in order to retrieve HCHO slant columns, (2) a background normalization procedure to eliminate remaining unphysical dependencies, and (3) the calculation of tropospheric air mass factors using radiative transfer calculations and modelled a priori profiles. In GOME-2 v12, two fitting intervals were introduced to improve the treatment of BrO absorption features, and to reduce the noise on the HCHO columns (328.5–359 nm for the pre-fit of BrO, 328.5–346 nm for the fit of HCHO) (De Smedt et al., 2012).

In the current version, a third fitting interval (339–364 nm) is used to pre-fit the O<sub>2</sub>-O<sub>2</sub> slant columns in order to minimize the effect of spectral interferences between the molecular absorptions. This results in a global reduction of the HCHO slant columns over the continents compared to the previous version, by 0 to 25%, depending on the season and the altitude. It is interesting to note that the effect is very similar when applied to GOME-2 and OMI HCHO retrievals, i.e. it has little or no impact on the diurnal variations (De Smedt et al., 2015). In order to improve the fit of the slant columns, an iterative DOAS algorithm for removal of spike residuals has been implemented (Richter et al., 2011). In addition, this version of the algorithm makes use of radiance spectra, daily averaged in the equatorial Pacific, which serve as reference spectra. The background normalisation now depends on the

615 day, the latitude, but also on the viewing zenith angle of the observation. This also serves as destripping procedure, needed for an imager instrument such as OMI (Boersma et al., 2011). The air mass factor calculation is based on Palmer et al. (2001). Scattering weighting functions are calculated with the LIDORT v3.3 radiative transfer model (Spurr, 2008).

The a priori profile shapes are provided by the IMAGES model, at 9h30 LT for GOME-2 and 13h30 LT for OMI (cf. Sect. 2). The OMI-based surface reflection database from Kleipool et al. (2008) is used for both GOME-2 and OMI. Radiative cloud effects are corrected using the independent pixel approximation (Martin et al., 2002) and the respective cloud products of the instruments provided by the TEMIS website (<http://www.temis.nl>), namely the GOME-2 O<sub>2</sub> A-band Frescov6 product (Wang et al., 2008) and the OMI O<sub>2</sub>-O<sub>2</sub> cloud product (Stammes et al., 2008). As for the previous algorithm versions, v14 HCHO columns are openly available on the TEMIS website (<http://h2co.aeronomie.be/>).

Monthly averaged HCHO columns from both instruments gridded onto the resolution of the model are used as top-down constraints. The simulated monthly averaged columns are calculated from daily values weighted by the number of satellite (OMI or GOME-2) measurements for each day at each model grid cell. Columns with a cloud fraction higher than 40% are excluded from the averages. HCHO data are also excluded over oceanic IMAGES gridcells (for which the land fraction is lower than 0.2), since we aim to constrain only continental sources, as well as in the region of the South Atlantic geomagnetic anomaly, i. e. within less than 1500 km of its assumed epicentre (47.0 W, 24.9 S). Finally, regridded columns for which the monthly and spatially averaged retrieval error exceeds 100% are also rejected. The error of the satellite columns is defined as the square root of the squared sum of the retrieval error and an absolute error of  $2 \cdot 10^{15}$  molec.cm<sup>-2</sup>. In most VOC-emitting regions the error ranges between 40% and 60%.

The monthly regridded HCHO columns from GOME-2 and OMI are shown in Fig. ?? for July 2010. As seen ~~on~~ in this figure, and discussed in De Smedt et al. (2015), the early afternoon columns of OMI are higher than the mid-morning values of GOME-2 at mid-latitudes, while the reverse is true at most tropical locations, in qualitative agreement with the

ground-based measurements and modelling results (Figs. ?? and ??).

## 5 ~~Overview of the results~~ Inversion methodology

~~Table 2 summarizes the source inversions carried out in this study. In each inversion, the emission rates of the three emission categories (anthropogenic, biogenic and biomass burning) are adjusted per month and per model grid.~~ The flux inversion technique consists in minimizing the mismatch between the model predictions and a set of chemical observations by adjusting the a priori emission distributions  $\Phi_i(x, t)$ , where  $(x, t)$  denote the spatial (latitude, longitude) and temporal (year, month, day) variables, and  $i$  the different emission categories (biogenic, pyrogenic, anthropogenic). We express the optimized solution  $\Phi_i^{opt}(x, t)$  as

$$\Phi_i^{opt}(x, t) = \sum_{j=1}^m e^{f_j} \Phi_i(x, t)$$

where  $\mathbf{f} = (f_j)$  is the vector of variables to be determined so as to minimize ~~a cost function measuring the overall bias between the model and a set of observations, i. e. the scalar function  $J$  (also termed as cost function)~~

$$J(\mathbf{f}) = \frac{1}{2} \text{tr} \left( 0.5 \left( (H(\mathbf{f}) - \mathbf{y})^T \mathbf{E}^{-1} (H(\mathbf{f}) - \mathbf{y}) + \mathbf{f}^T \mathbf{B}^{-1} \mathbf{f} \right) \right) \text{tr} 0.5$$

660 which measures the discrepancy between the modelled HCHO columns  $H(\mathbf{f})$  and the observations  $\mathbf{y}$ . In this expression <sup>T</sup> is the transpose of the matrix,  $\mathbf{E}$  and  $\mathbf{B}$  are the matrices of errors on the observations  $\mathbf{y}$  and on the variables  $\mathbf{f}$ , respectively. The gradient of the cost function  $J$  with respect to the input variables ( $\partial J / \partial \mathbf{f}$ ) is calculated using the adjoint of the model. A thorough description of the method and its implementation in the IMAGESv2 CTM is given in Müller and Stavrakou (2005); Stavrakou et al. (2009b). The inversion is performed at the model resolution ( $2^\circ \times 2.5^\circ$ ) using an iterative algorithm suitable for large scale problems (Gilbert and Lemaréchal, 1989)

665 The source inversions presented in Table 2 infer the emission rates of the three emission categories (anthropogenic, biogenic and biomass burning) are adjusted per month and are constrained by either GOME-2 or OMI

HCHO columns. On the global scale, ca. 63,000 flux parameters are varied. The emission of a grid cell is not optimized when its maximum a priori monthly value is lower than  $10^{10}$  molec.cm<sup>-2</sup> s<sup>-1</sup>. The assumed error on the a priori anthropogenic emission by country is set equal to a factor 1.5 and 2 for OECD and other countries, respectively, to a factor of 2 for biogenic emissions and 3 for fire burning emissions - ~~More details about the inversion framework can be found in~~ (Stavrakou et al., 2009b).

The sensitivity studies (Table 2) aim at assessing the impact of (i) the choice of a priori errors on the emission fluxes (OMI-DE, OMI-HE), (ii) the cloud fraction filter applied to the satellite data (OMI-CF), and (iii) the isomerization of isoprene peroxy radicals (OMI-IS). The annual a priori and top-down fluxes of the two standard and the four sensitivity inversions are summarized in Table 3. The a priori model columns calculated at 9h30 and 13h30 local time are generally higher than the GOME-2 or OMI HCHO column abundances (Fig. ??), e. g. over Europe, Southern China, the United States, Amazonia and Northern Africa. They are however found to agree generally well in terms of seasonality (Fig. ??).

## 6 Overview of the results

Globally, the cost function is reduced by a factor of 2 after optimization, and its gradient is reduced by a factor of ca.  $10^3$ . In general, the consistency between the two inversions is ~~found to be~~ highest in tropical regions. At mid-latitudes, the emission updates (i.e. the ratios of optimized to prior emissions) are almost systematically higher in the OMI-based than in the GOME-2-based inversion. This reflects ratios of 13h30 to 9h30 columns which are lower in the model than suggested by the two satellite datasets.

Both GOME-2 and OMI inversions suggest a strong decrease in global biomass burning VOC emissions with regard to the a priori GFEDv3 inventory, by 36% and 33%, respectively. This decrease is most pronounced in tropical regions. In contrast, both the OMI and GOME-2 optimizations lead to enhanced emissions (by about 50%) due to the extensive fires which plagued European Russia in August 2010 (Sect. 7.2) and to agricultural waste burning in the North

China Plain in June (Sect. 7.3). The fire burning estimates from the two base inversions are generally quite consistent, not only globally but also over large emitting regions like Amazonia, Southeastern Asia, and Africa. The sensitivity studies provide global flux estimates which are close (within 7%) to the standard top-down results using OMI.

The globally derived isoprene fluxes are reduced in both standard inversions, by 9% according to GOME-2 and by 13% according to OMI, compared to the a priori estimate of the MEGAN-ECMWF-v2 inventory (363.1 Tg/yr, Table 3). The overall consistency between the global estimates is high for this emission category, despite some significant differences at a regional scale (cf. next sections). The biogenic top-down fluxes derived from the sensitivity inversions of Table 2 lie within 5% of the OMI-based estimates on the global scale, yet larger differences are found in the regional scale.

Finally, the global anthropogenic source is decreased in the GOME-2 inversion, while it is slightly increased in the inversion using OMI. Despite their limited capability to constrain this emission category on the global scale due to its small contribution to the global HCHO budget (Stavrakou et al., 2009a), the satellite observations are found to provide constraints over highly polluted regions, notably Eastern China, where however the discrepancy between the two sensors is most evident (see Sect. 7.3).

Annual emission updates for the different source categories, and the monthly variation of the a priori and optimized flux estimates are illustrated in Figs. ??, ??, ??, ?? and ??.

Modifying the errors on the flux parameters infers global isoprene emission decreases of ca. 15% (OMI-HE) and 30% (OMI-DE) with regard to the initial isoprene inventory, and within 7% of the standard OMI inversion, cf. Table 3. As expected, due to the limited or stronger confidence assigned to the a priori inventories in OMI-DE and OMI-HE scenarios, respectively, most substantial departures from the a priori inventory are obtained when doubling the errors on the emission parameters, while the OMI-HE scenario lies closer to the a priori database. The impact of the use of a stricter cloud criterion on the OMI scenes used as top-down constraints (20% for OMI-CF instead of 40% in OMI base inversion) results in weak increases of the globally inferred

fluxes with respect to the OMI inversion, but the enhancement is ~~found to be~~ more important in extratropical regions, and amounts to 22% for biomass burning emissions (Table 3, ~~and left panel of Fig. ??~~). Finally, suppressing the isomerization channel in isoprene oxidation increases the HCHO yield from isoprene and leads to slightly higher model columns over isoprene-rich regions. ~~The As seen on the right panel of Fig. ??, the~~ resulting isoprene fluxes are ~~found to be only~~ slightly lower compared to the reference run (by 4% lower on the global scale, ~~but over Amazonia, the emission reduction is estimated at~~). ~~Over Amazonia, this emission reduction reaches~~ 8% ~~compared to the results of OMI inversion~~.

## 7 Emissions at the mid-latitudes

### 7.1 North America

Biogenic isoprene emissions drive the HCHO column seasonality and explain the summertime column peak in the Eastern US (Fig. ??). The a priori model exhibits, however, a much stronger seasonal variability than the observation with a summer-to-winter ratio of 4-5 compared to the observed ratio of about 2. In summertime, the a priori model overestimates the GOME-2 and OMI measurements by up to 50% and 35%, respectively in the Eastern US (Figs. ?? and ??). This drives the significant decrease in the optimized isoprene fluxes, from the a priori value of 17.8 Tg to 11.6 Tg (GOME-2) and to 13.8 Tg (OMI) over the US in 2010, in good agreement with our earlier flux estimates (13 Tg/yr) based on SCIAMACHY HCHO columns (Stavrakou et al., 2009b). Even larger reductions are found in the Southeastern US, amounting to ca. 25% and 40% in the OMI and GOME-2 inversions, respectively (Fig. ??). Anthropogenic and pyrogenic emissions over the US are essentially unchanged by the inversions.

The estimated cumulative June-August US isoprene emissions from both optimizations (7.8 Tg for GOME-2 and 9.5 Tg for OMI) agree well with reported values based on earlier versions of OMI HCHO retrievals (9.3 Tg according to the variable slope technique as described in Millet et al. (2008)). The OMI-based isoprene flux in July 2010, estimated at 3.23 Tg, is by 30% lower than the a priori (4.62 Tg), corroborating the low values of the BEIS2 inventory (Palmer et al., 2003).

The model predictions are compared to HCHO measurements from the INTEX-A aircraft campaign conducted in July-August 2004 over the Eastern US (Singh et al., 2006; Fried et al., 2008) in Fig. ??). It is worth noting that the measurements by NCAR (National Center for Atmospheric Research) and URI (Univ. Rhode Island) exhibit large differences between them, the NCAR values being by ca. 50% higher than URI below 2 km altitude (Fig. ??). The model simulations are performed for 2004, and the concentrations are sampled at the locations and times of the airborne measurements. In the a posteriori simulation shown in Fig. ??, the bottom-up isoprene emissions for 2004 were multiplied by the isoprene emission update inferred from either the OMI or the GOME-2 inversion for 2010. As seen ~~on~~ in Fig. ??, the average HCHO concentration below 2 km altitude is decreased by about 10% in the OMI inversion (15% in the case of GOME-2) and remains within the range of the NCAR and URI measurements. Despite the marked underestimation of the modelled HCHO (1.39 and 1.32 ppbv in the OMI and GOME-2 inversions) in comparison to NCAR observations (1.83 ppbv), the emission optimization results in an increased Pearson's spatial correlation coefficient between the modelled and observed concentrations below 2 km, from 0.74 in the a priori to 0.79 and 0.80 in the OMI and GOME-2 inversions. A similar improvement is found with respect to URI data.

### 7.2 Russia

The a priori model underpredicts the observed OMI HCHO columns during the Russian fires of July-August 2010 by up to a factor of 2, in particular over a broad region extending to the North (61 N) and East (55 E) of Moscow (Fig. ??, upper panel). Similar spatial patterns are also observed in GOME-2 HCHO columns. However, the GOME-2 columns are lower than OMI over this region, and the model underestimation is less severe in this case reaching 60%. The lower GOME-2 values might be due to the lower retrieval sensitivity of GOME-2 to lower tropospheric HCHO compared to OMI at these latitudes, associated to larger solar zenith angles (De Smedt et al., 2015). As a result, the increase of the pyrogenic emission fluxes is strongest in the OMI inversion, from 440 Gg VOC in the GFEDv3 inventory, to 720 Gg VOC (630 Gg VOC in GOME-2) in August 2010 over Europe. Accord-

ingly, the isoprene fluxes inferred from the OMI inversion in August are also larger, about 40% higher than the a priori estimate in the Moscow area, whereas the increase derived by GOME-2 does not exceed 25%. Overall, the OMI data suggest annual isoprene fluxes in Europe by 11% higher than the a priori inventory (Table 3).

Strongly enhanced fire emissions in the Moscow region between mid-July and mid-August 2010 were reported based on satellite observations of CO from MOPITT (Konovalov et al., 2011) and IASI (Krol et al., 2013; R'honi et al., 2013), and on surface ~~measurements~~ measurements (Konovalov et al., 2011). The optimized fire emission inferred by assimilation of IASI CO columns in Krol et al. (2013) lies within 22 and 27 Tg CO during the fires, i.e. about 7-10 times higher than in the bottom-up inventory (GFEDv3). These values are comparable with the ranges of 19-33 and 34-40 Tg CO suggested by R'honi et al. (2013) and Yurganov et al. (2011), respectively, but are much higher than reported values of ca. 10 Tg CO derived using surface CO measurements in the Moscow area (Konovalov et al., 2011). The latter study identifies the contribution of peat burning to the total CO fire emission in this region to be as high as 30%.

The IMAGESv2 a priori CO simulation (using GFEDv3 inventory) underestimates substantially the IASI CO observations. Scaling the CO emissions in IMAGESv2 to the fire VOC increase suggested by the OMI HCHO optimization, i.e. ca. 60% in July and August 2010, barely improves the model agreement with the satellite, indicating that, in accordance with earlier studies, more drastic fire flux enhancements (factor of 5 to 10) are required to reconcile CO model-data mismatches. The reasons for the differences in the emission increases inferred by CO and HCHO during the 2010 Russian fires are currently unknown, but could be related either to inadequate knowledge of emission factors of CO and VOCs from peat fires, and/or underestimated remote-sensed HCHO columns over fire scenes due to possibly important aerosol effects not accounted for in the retrievals.

### 7.3 China

The dominant emission source in China is anthropogenic and is estimated at 25.5 TgVOC in REASv2 (Kurokawa et al., 2013) for 2008. The biogenic source, mainly located in

Southern China, amounts to 7 Tg in 2010 in the MEGAN-MOHYCAN-v2 inventory (Stavrakou et al., 2014; Guenther et al., 2006, 2012). In Northern China, the HCHO columns are underestimated by the a priori model in winter compared to OMI, whereas a relatively good agreement is found in summer. In Southern China, a general model overestimation is found all year round (Figs. ?? and ??).

Although the OMI-based inversion yields total Chinese anthropogenic emissions very similar to the a priori (24.6 TgVOC), the emission patterns are modified with increased emissions in Northeast China and especially around Beijing (20-40%), and emission reductions in the Southeast and in particular around Shanghai (15-47%) and Guangzhou (15-30%). The total GOME-2 emission, estimated at 20.6 TgVOC, is lower than the OMI result, but in good agreement with the estimate (20.2 Tg in 2008) of the Multi-resolution Emission Inventory for China (MEIC, <http://www.meicmodel.org>). The flux distributions from both inversions have common features, e.g. decreased fluxes in Shanghai and Guangzhou regions, but contradicting estimates in the Northeast where GOME-2 observations do not support the emission enhancements suggested by OMI.

This discrepancy is primarily due to the lower modelled ratios of 13h30 to 9h30 columns (average ratio of 1.0 in the model in North China between March and November) compared to the satellite datasets (Fig. ?? average ratio of 1.16). Note that, however, the model was found to overestimate this ratio against MAX-DOAS data at Beijing and Xianghe (Fig. ??). Another possible cause for difference between the OMI and GOME-2 results is the limited availability of GOME-2 data in wintertime (Fig. ??) due to the high solar zenith angles leading to large retrieval errors frequently exceeding 100%. For example, GOME-2 columns are unavailable from November to April over Beijing.

In the North China Plain, one of the largest agricultural plains on Earth, the post wheat harvest season fires set up every year in June is a common farmer's practice (Huang et al., 2012), responsible for poor air quality conditions and environmental harm (Yamaji et al., 2010). Both OMI and GOME-2-based inversions suggest a considerable enhancement of the agricultural fire flux in this region, by almost a factor of 2 in comparison with the a priori inventory by

Huang et al. (2012), cf. Fig. ??). The interannual variability of these emissions will be addressed in a separate work in preparation.

Finally, the Chinese isoprene emission are decreased from 7 Tg per year to 6.5 Tg (OMI) and 5.9 Tg (GOME-2), with especially strong decreases in Southern China, as illustrated in Fig. ??.

## 8 Emissions in the Tropics

### 8.1 South America

After the 2005 drought in Amazonia, characterized as one-in-a-century event (Marengo et al., 2008), Amazonia suffered a second, even more severe drought in 2010 with major environmental impacts (Marengo et al., 2011). Extensive wildfires broke out in different regions from July to October, with central and south Amazonia as main epicenters. The massive fire burning is reflected in the high HCHO columns (up to  $15 \cdot 10^{15}$  molec.cm<sup>-2</sup>) detected by GOME-2 and OMI during these months, about twice the observed columns in the wet season (Fig. ??). Both instruments agree very well on the magnitudes and spatial patterns of the HCHO columns, as illustrated in Fig. ??). The a priori model strongly overestimates the observations during the dry season (by up to 70% in August) indicating that the GFEDv3 emissions for this region are most likely too high. The GOME-2 and OMI inversions decrease the fire emission by factors of 2 and 2.5, respectively (Fig. ??). Even stronger decreases (factor of 3) are found over Northern Bolivia and central Amazonia (Fig. ??).

These emission reductions are supported by comparison with CO columns observed by ~~the Infrared Atmospheric Sounding Interferometer (IASI) instrument on the MetOp payload~~ IASI (George et al., 2009). The use of fire emissions from GFEDv3 leads to strongly overestimated CO columns in comparison to IASI observations in August 2010 (Fig. ??), reaching almost a factor of 2 over Western Amazonia. Significant improvement in the model-data match is achieved when the emission reduction inferred by the OMI-based inversion is implemented and applied not only to NMVOCs but also to other compounds including CO. The GFEDv3 emissions of CO in 2010 were also found to be substantially overestimated, by a factor of  $\sim 1.8$  over South America between 5°S

and 25°S, by inverse modelling of MOPITT CO columns using the GEOS-Chem model (Bloom et al., 2015). The most likely cause for the lower emissions in 2010 compared to 2007 was proposed by these authors to be a reduction of the combusted biomass density possibly due to dry conditions and/or repeat fires. The good consistency found between results using either CO or HCHO indicates that the emission factors used in the model for NMVOC and CO (or at least their ratios) are appropriate, unless an error compensation is responsible for the noted good agreement. Note also that, besides the good consistency found between the emission estimates derived from GOME-2 and OMI, the performed sensitivity inversions induce only very weak departures from the standard inversion (Fig. ??).

Isoprene fluxes over Amazonia derived by GOME-2 and OMI inversions are ~~estimated at 73.7 Tg and 92.5 Tg~~ equal to 92.5 Tg and 73.7 Tg, respectively. This is by 25% and 7% lower than the prior and in good agreement with previous studies using satellite HCHO observations from the SCIAMACHY instrument (Stavrakou et al., 2009b). The seasonal variation of the posterior fluxes is ~~found to be~~ consistent with the a priori inventory, except during the transitional wet-to-dry period (April-June) with both GOME-2 and OMI satellite datasets pointing to a significant flux decrease by ca. 25% (Fig. ??). This behaviour confirms previous comparisons using GOME HCHO observations suggesting that factors other than the temperature influence the observed variability (Barkley et al., 2008), such as the growth of new leaves causing a temporary shut-down of the emissions (Barkley et al., 2009).

### 8.2 Indonesia

Fire activity was exceptionally low in 2010, with annual emissions of about 0.1 TgVOC, i. e. about two orders magnitude less than for high years such as 2006 according to GFEDv3.

The GOME-2 and OMI inferred isoprene estimates show good consistency over Indonesia all year round, amounting to 10.3 Tg and 11.1 Tg, respectively, close to the a priori (11.6 Tg). The inferred isoprene emissions are, however, twice lower than reported fluxes of 25 Tg/yr based on SCIAMACHY HCHO observations, which were themselves de-

creased with respect to their priori isoprene flux of 35 Tg/yr (Stavrou et al., 2009b). In comparison to that study, the isoprene a priori emissions used in the present work are strongly reduced over this region, due to a drastic reduction by a factor of 4.1 of the MEGANv2.1 basal isoprene rate for tropical rainforests over Asia, as suggested by field measurements in Borneo (Langford et al., 2010). This reduction implemented in the MEGAN-MOHYCAN-v2 model (Stavrou et al., 2014) is found here to be corroborated by GOME-2 and OMI HCHO measurements.

### 8.3 Indochina

The Northern part of the Indochinese peninsula (primarily Myanmar, also Assam in India and parts of Thailand) faces intense forest fires during the dry season, as very well seen in the GOME-2 and OMI HCHO timeseries, with values reaching  $15 \cdot 10^{15} \text{ molec.cm}^{-2}$  in March, about three times higher than in the wet season (Fig. ??).

Both the GOME-2 and OMI data point to substantial, but very ~~contrasted~~ contrasting updates in the pyrogenic fluxes during the fire season (March, Fig. ??): flux reductions by a factor of 2–5 over Myanmar and surrounding forested areas, and flux increases by a factor of almost 2 (or more in the case of OMI) over the Southeastern part of the peninsula, which includes Cambodia, Southern Laos and Southern Vietnam. In the OMI-DE inversion assuming doubled errors on the a priori fluxes, the updates are even more pronounced and reach a factor of 4 over parts of Vietnam and Laos. The annual emissions in the entire region are decreased by 15% and 26% ~~in~~ according to the OMI and GOME-2 inversions, respectively. As illustrated in Fig. ??, the optimization leads to a substantial improvement of the model performance, although the HCHO columns remain significantly underestimated (by up to 20%) in the Southern part of the peninsula (e. g. Cambodia), most likely due to a too strong underestimation of the GFEDv3 emissions used as a priori in the model. The emission drop over Myanmar and the need for higher emissions in the Southeast are partly confirmed by comparisons with IASI CO columns. Indeed, as seen on the lower panel of Fig. ??, modelled CO simulations using ~~either GFEDv3 or~~ biomass burning fluxes optimized using OMI data (Fig. ?? i.e. reduced by ca. 26% in March relative

to GFEDv3) display a better agreement ~~in the second case with the observed CO columns~~, despite an underestimation ~~of CO by ca.~~ by  $\sim 10\%$  over most of the peninsula. This result is consistent with the moderate reduction (ca. 20% in March) of biomass burning emissions of CO over Tropical Asia inferred by Basu et al. (2014)

The strong enhancement of pyrogenic emissions required to comply to the satellite data over the Southeastern part of Indochina might be due to the occurrence of agricultural fires in those regions (e. g. Cambodia), known to be a common management practice (Chang and Song, 2010). These fires are very difficult to detect by satellite due to their limited spatial extent. It is worth noting that the latest version of the Fire Inventory from NCAR (Wiedinmyer et al., 2011) (FINNv1.5) predicts much higher emissions from this region : ca. 43 TgC in March in the region 100–108 E, 10–18 N, i.e. a factor of 10 higher than in the GFEDv3 inventory (4.3 TgC). The differences between GFEDv3 and FINN are most likely due to inherent differences in the proxy variables used in the respective emission models, burned area in the case of GFEDv3, and active fire counts in FINN model, both retrieved from MODIS satellite data. The two inventories provide however very similar estimates for the more forested, Northwestern part of Indochina (19–27 N, 97–100 E): 105 TgC in GFEDv3, 124 TgC in FINNv1.5.

Considerable cloudiness during the rainy season (May–October) causes gaps in the OMI HCHO timeseries, due to the exclusion of scenes with  $\geq 40\%$  cloud cover. The GOME-2 data series are comparatively less affected by this issue, due to the diurnal precipitation and cloudiness patterns during the monsoon season. Indeed, long-term observations over Indochina (Takahashi et al., 2010) reveal an early afternoon rainfall peak (13–16h LT), and heavy rainfall in the early morning (4–7h), but lower precipitation rates between 7 and 10h. GOME-2 observations are therefore less contaminated by clouds and offer a better spatial coverage during the rainy season in this region.

### 8.4 Africa

Over Africa, the annual pyrogenic source, amounting at 40.7 TgVOC in the a priori, is reduced to 26.2 and 32.6 TgVOC in the GOME-2 and OMI inversions, respectively (Table 3).



1085 A smaller reduction is also inferred for isoprene fluxes, es-  
timated at 76.6 Tg (GOME-2) and at 74.2 Tg (OMI), within  
10% of the a priori value (81.6 Tg). These estimates are in  
line with recently reported isoprene fluxes over Africa based  
1090 on the NASA dataset of OMI HCHO columns (77 Tg C or  
87 Tg isoprene compared to 116 Tg isoprene in the a priori,  
Marais et al. (2012)). The spatial distribution of the emission  
updates is displayed in Figs. ??, ?? and ??.

African fire occurrence peaks in central Africa (e. g., the  
Democratic Republic of the Congo or DRC) in early June  
1095 (Fig. ??) and lasts until August with the end of the dry sea-  
son. The GOME-2 and OMI observations show an excel-  
lent accordance, with morning columns being about 10%  
higher than in the afternoon, consistent with measurements  
in Bujumbura (Fig. ??), although the morning-to-afternoon  
1100 ratio was found to be higher in the ground-based observa-  
tions (1.25). The model simulations overpredict the ob-  
servations of both sounders during the fire season by 10-  
25%. The posterior bias reduction (cf. Fig. ??, DRC region)  
is achieved by a significant biomass burning flux decrease,  
1105 reaching a factor of 2 in the southern part of DRC, and 20-  
30% elsewhere between 2 and 12°S. In a similar manner,  
up to a factor of 2 emission decrease is also needed in the  
region of the Central African Republic during the fire sea-  
son (November-February) to match the observed columns  
1110 (Fig. ??), in good agreement with our previous study us-  
ing SCIAMACHY HCHO columns (Stavrakou et al., 2009b).  
Only small changes are inferred for isoprene emissions in  
Northern Africa, by 11% (GOME-2) and by 16% (OMI) de-  
crease compared to the a priori, as illustrated in Fig. ??.

1115 In Southern Africa, biogenic fluxes are highest in January<sup>1155</sup>  
and lowest in July, while the fire season starts in May, and  
peaks in September (Figs. ?? and ??). Both GOME-2 and  
OMI inversions infer only small isoprene flux updates (Ta-  
ble 3). Regarding fire emissions, in contrast with GOME-2  
1120 data suggesting a ca. 30% flux reduction (to 17.6 from 25.8<sup>1160</sup>  
TgVOC), the OMI-based estimate lies within 10% of the a  
priori, due to a compensation of flux decreases North of ap-  
prox. 15 S, and flux increases in the southernmost part of  
the continent, south of ca. 15 S (Fig. ??). Although the sea-  
1125 sonal patterns are essentially preserved by the optimization,<sup>1165</sup>  
both inversions predict higher emissions at the end of the dry

season, especially over Zambia and surrounding regions (Oc-  
tober, Fig. ??). These updates are highest (factor of ~2) in  
the OMI optimization, but the patterns are very similar in  
both inversions.

## 9 Conclusions

The emissions of NMVOCs in 2010 were optimized by in-  
verse modelling using the IMAGESv2 CTM and its adjoint  
with HCHO column abundances from either GOME-2 or  
OMI as observational constraint. Given their different over-  
pass times, the consistency of the inferred emissions depends  
on how the model can faithfully reproduce the diurnal cycle  
of HCHO columns. The modelled diurnal cycle displays a  
great variability mirroring the competing influences of pho-  
tochemical productions and losses as well as the diurnal pro-  
files of emissions and (to a lesser extent) meteorological pa-  
rameters. Where anthropogenic VOCs are dominant, day-  
time photochemical production and the anthropogenic emis-  
sion profile leads to an early afternoon maximum, in agree-  
ment with MAX-DOAS observations in Belgium, Holland and  
(during summertime) the Beijing area. Over oceanic ar-  
eas, where methane oxidation is the only significant source  
in the model, a similar behavior is also simulated, in agree-  
ment with FTIR data at Reunion Island. The poor model  
performance at several locations (Bujumbura, OHP, Beijing  
in winter/spring) is likely at least partly due to the coarse  
model resolution, as shown by the very different diurnal pro-  
files observed at Beijing and Xianghe. This limited repre-  
sentativity of local ground-based sites possibly explains (part  
of) the large deviations (typically  $\pm 10\text{-}30\%$ ) found between  
the calculated and observed ratios of the HCHO columns at  
13h30 and 9h30. Despite this large scatter, the average ra-  
tio of 13h30 columns to 9h30 columns is only slightly higher  
(1.126) in the model compared to the MAX-DOAS and FTIR  
measurements (1.043).

Unfortunately no ground-based measurements are avail-  
able in regions where the simulated diurnal cycle amplitude  
is largest, namely over intense fire scenes at both tropical and  
boreal latitudes. Over these regions, an evening maximum is  
predicted, and the peak-to-trough ratio reaches up to 70%. In  
isoprene-rich areas, the diurnal HCHO cycle often, but not

always, displays a minimum around noon, when the photochemical sink is highest, and a maximum in the late evening or early morning, in agreement with a previous modelling study (Barkley et al., 2011). Validation studies over forested areas will be needed to determine how realistic these patterns are.

The ratio of 13h30 to 9h30 column is ~~found to be~~ most often between 0.8 and 1.2 according to ground-based measurements. Similar, but generally higher values of this ratio are calculated by the model, by 8% on average. The satellite, on the other hand, although in qualitative agreement with the above, suggests higher ratios of 13h30 to 9h30 columns than the model at mid-latitudes, whereas no clear pattern emerges in tropical regions (Fig. ??). Nevertheless, these discrepancies in terms of morning/afternoon ratios are most often small in comparison with the model/data differences in the HCHO columns themselves. As a consequence, the emission fluxes inferred from both GOME-2 and OMI inversions are found to be generally very consistent. They both suggest a strong decrease of the global biomass burning source, by about 35%. The decrease is mostly concentrated in the Tropics, e.g. over Amazonia (factor of  $>2$  reduction) over Equatorial Africa and over Myanmar and surrounding regions (factor of 2–5 reduction in March). These updates are confirmed by comparing CO columns predicted by the model using the biomass burning emissions estimated by the OMI inversion with IASI CO columns. The results are also consistent with a recent study using MOPITT CO columns (Bloom et al., 2015). The seasonal profile of the emissions is generally well preserved by the inversions, except for a significant enhancement near the end of the dry season, in particular over Southern Africa (in October) but also Amazonia (in September) and Indochina (in April). Both satellite datasets point to strong enhancements of agricultural fire fluxes in the North China Plain in June (factor of almost 2) and in the southern part of Indochina, compared to the a priori estimate.

Very good agreement between the inversion results is found for isoprene fluxes, with global annual fluxes reduced by 9% (GOME-2) and 13% (OMI) compared to the a priori of 363 Tg. In the Southeastern US, both inversions agree on a substantial decrease by ca. 25% (OMI) and 40% (GOME-2)

in good agreement with previous estimates based on SCIAMACHY and OMI HCHO data. This reduction improves the correlation between calculated and observed HCHO concentrations during the airborne INTEX-A campaign conducted over the Eastern US. Over Amazonia, the source of isoprene is ~~found to be~~ consistently lower than the a priori, in particular during the wet-to-dry season transition (April–June), in accordance with previously reported estimates. Over Indonesia, the optimizations do not present significant deviations from the prior, thereby validating the a priori isoprene inventory which incorporated decreased basal emission rates for Asian tropical rainforests.

The results show that the global anthropogenic VOC fluxes are not well constrained, as indicated by the negligible updates derived by the inversions over most areas, except over highly polluted regions with a distinct anthropogenic signal in the HCHO columns, like China. In this region, the changes in the emission patterns found by the OMI-based optimization are not well reproduced by the inversion of GOME-2 data, likely reflecting discrepancies in the 13h30/9h30 column ratio calculated by the model. In spite of those discrepancies, our study demonstrates that a high degree of compatibility is achieved between top-down pyrogenic and biogenic emissions derived by GOME-2 and OMI HCHO data, while the flux estimates are found to be weakly dependent to changes in key uncertain parameters in the performed sensitivity inversions.

This study identifies several important large regions where the differences between bottom-up and top-down estimates are particularly important and the inferred flux estimates from both satellites show a high degree of consistency, like the Amazon and the Southeast US. Recent airborne field measurements in those regions should provide additional constraints and help close the gap between bottom-up and top-down estimates. The increasing availability of in-situ observations of formaldehyde and related trace gases can provide a basis for improving and assessing model simulations of diurnal variations over a range of environmental conditions and interactions between biogenic and anthropogenic compounds (e.g. DiGangi et al. (2012)). Furthermore, planned geostationary satellites have the potential to improve satellite based emission estimates by characterizing

diurnal variations in atmospheric constituents (Saide et al., 2014). Finally, new cross section measurements of isoprene<sup>295</sup> in the infrared open new avenues for the detection of isoprene using satellite (e.g. IASI) and a direct link to isoprene emission (Brauer et al., 2014).

*Acknowledgements.* This research was supported by the Belgian<sup>300</sup> Science Policy Office through the PRODEX projects ACROSAT and IASI.Flow (2014-2015), and by the European Space Agency (ESA) through the GlobEmission project (2011-2016). P.-F.C. is senior research associate with FRS-FNRS.

## References

- Andreae, M.O., and P. Merlet : Emission of trace gases and aerosols from biomass burning, *Global Biogeochem. Cy.*, 15(4), 955–966, doi:10.1029/2000GB001382, 2001. <sup>1310</sup>
- 1265 Arneth, A., G. Schurgers, J. Lathièrre, T. Duhl, D. J. Beerling, C. N. Hewitt, M. Martin, and A. Guenther : Global terrestrial isoprene emission models: sensitivity to variability in climate and vegetation, *Atmos. Chem. Phys.*, 11, 8037–8052, doi:10.5194/acp-11-8037-2011, 2011. <sup>1315</sup>
- 1270 Barkley, M. P., P. I. Palmer, U. Kuhn, J. Kesselmeier, K. Chance, T. P. Kurosu, R.V. Martin, D. Helmig, and A. Guenther : Net ecosystem fluxes of isoprene over tropical South America inferred from Global Ozone Monitoring Experiment (GOME) observations of HCHO columns, *J. Geophys. Res.*, 113, D20304, doi:10.1029/2008JD009863, 2008. <sup>1320</sup>
- 1275 Barkley, M. P., P. I. Palmer, I. De Smedt, T. Karl, A. Guenther, and M. Van Roozendaal : Regulated large-scale annual shut-down of Amazonian isoprene emissions? *Geophys. Res. Lett.*, 36, L04803, doi:10.1029/2008GL036843, 2009. <sup>1325</sup>
- 1280 Barkley, M. P., P. I. Palmer, L. Ganzeveld, A. Arneth, D. Hagberg, T. Karl, A. Guenther, F. Paulot, P. O. Wennberg, J. Mao, T. P. Kurosu, K. Chance, J.-F. Müller, I. De Smedt, M. Van Roozendaal, D. Chen, Y. Wang, and R. M. Yantosca : Can a “state of the art” chemistry transport model simulate Amazonian tropospheric chemistry? *J. Geophys. Res.*, 116, D16302, doi:10.1029/2011JD01589, 2011. <sup>1330</sup>
- 1285 Bloom, A. A., J. Worden, Z. Jiang, H. Worden, T. Kurosu, C. Frankenberg, and D. Schimel : Remote sensing constraints on South America fire traits by Bayesian fusion of atmospheric and surface data, *Geophys. Res. Lett.*, accepted for publication, doi: 10.1002/2014GL062584, 2015. <sup>1335</sup>
- Bloss, C., V. Wagner, A. Bonzanini, M. E. Jenkin, K. Wirtz, M. Martin-Reviejo, and M. J. Pilling : Evaluation of detailed aromatic mechanisms (MCMv3 and MCMv3.1) against environmental chamber data, *Atmos. Chem. Phys.*, 5, 623–639, 2005.
- Boersma, K. F., H. J. Eskes, R. J. Dirksen, R. J. van der A, J. P. Veefkind, P. Stammes, V. Huijnen, Q. L. Kleipool, M. Sneep, J. Claas, J. Leitão, A. Richter, Y. Zhou, and D. Brunner : An improved tropospheric NO<sub>2</sub> column retrieval algorithm for the Ozone Monitoring Instrument, *Atmos. Meas. Tech.*, 4, 1905–1928, 2011.
- Brauer, C. S., T. A. Blake, A. B. Guenther, S. W. Sharpe, R. L. Sams, and T. J. Johnson : Quantitative infrared absorption cross sections of isoprene for atmospheric measurements, *Atmos. Meas. Tech.*, 7, 3839–3847, 2014.
- Chance, K., P. I. Palmer, R. J. D. Spurr, R. V. Martin, T. Kurosu, and D. J. Jacob : Satellite observations of formaldehyde over North America from GOME, *Geophys. Res. Lett.*, 27, 3461–3464, 2000.
- Chang, D., and Y. Song : Estimates of biomass burning emissions in tropical Asia based on satellite-derived data, *Atmos. Chem. Phys.*, 10, 2335–2351, 2010.
- Choi, W., I. C. Faloona, N. C. Bouvier-Brown, M. McKay, A. H. Goldstein, J. Mao, W. H. Brune, B. W. LaFranchi, R. C. Cohen, G. M. Wolfe, J. A. Thornton, D. M. Sonnenfroh, and D. B. Millet : Observations of elevated formaldehyde over a forest canopy suggest missing sources from rapid oxidation of arboreal hydrocarbons, *Atmos. Chem. Phys.*, 10, 8761–8781, doi:10.5194/acp-10-8761-2010, 2010.
- Crounse, J. D., F. Paulot, J. G. Kjaergaard, and P. O. Wennberg: Peroxy radical isomerization in the oxidation of isoprene, *Phys. Chem. Chem. Phys.*, 13, 13607–13613, 2011.
- Damian, V., A. Sandu, M. Damian, F. Potra, and G. R. Carmichael : The Kinetic PreProcessor KPP - A Software Environment for Solving Chemical Kinetics, *Comput. Chem. Eng.*, 26, 1567–1579, 2002.
- De Smedt, I., M. Van Roozendaal, T. Stavrakou, J.-F. Müller, C. Lerot, N. Theys, P. Valks, N. Hao, and R. van der A : Improved retrieval of global tropospheric formaldehyde columns from GOME-2/MetOp-A addressing noise reduction and instrumental degradation issues, *Atmos. Meas. Tech.*, 5, 2933–2949, 2012.
- De Smedt, I., T. Stavrakou, F. Hendrick, T. Danckaert, T. Vlemmix, G. Pinardi, N. Theys, C. Lerot, J.-F. Müller, P. Veefkind, M. Van Roozendaal : Diurnal, seasonal and long-term variations of global formaldehyde columns inferred from combined OMI and

- GOME-2 observations, submitted to *Atmos. Chem. Phys.*, 2015.
- DiGangi, J. P., S. B. Henry, A. Kammrath, E. S. Boyle, L. Kaser, R. Schnitzhofer, M. Graus, A. Turnipseed, J.-H. Park, R. J. Weber, R. S. Hornbrook, C. A. Cantrell, R. L. Maudlin, S. Kim, Y. Nakashima, G. M. Wolfe, Y. Kajii, E. C. Apel, A. H. Goldstein,<sup>1390</sup>  
 1345 A. Guenther, T. Karl, A. Hansel, and F. N. Keutsch : Observations of glyoxal and formaldehyde as metrics for the anthropogenic impact on rural photochemistry, *Atmos. Chem. Phys.*, 12, 9529–9543, doi:10.5194/acp-12-9529-2012, 2012.
- Dufour, G., F. Wittrock, M. Camredon, M. Beekmann, A. Richter,<sup>1395</sup>  
 1350 B. Aumont, and J. P. Burrows : SCIAMACHY formaldehyde observations: constraint for isoprene emission estimates over Europe? *Atmos. Chem. Phys.*, 9, 1647–1664, doi:10.5194/acp-9-1647-2009, 2009.
- Fried, A., J. G. Walega, J. R. Olson, J. H. Crawford, G. Chen,<sup>1400</sup>  
 1355 P. Weibring, D. Richter, C. Roller, F. Tittel, B. G. Heikes, J. A. Snow, H. Shen, D. W. O’Sullivan, M. J. Porter, H. E. Fuelberg, J. J. Halland, and D. B. Millet : Formaldehyde over North America and the North Atlantic during the summer 2004 INTEX campaign : Methods, observed distributions<sup>1405</sup>  
 1360 and measurement comparisons, *J. Geophys. Res.*, 113, D10302, doi:10.1029/2007JD009185, 2008.
- George, M., C. Clerbaux, D. Hurtmans, S. Turquety, P.-F. Coheur,<sup>1410</sup>  
 1365 M. Pommier, J. Hadji-Lazaro, D. P. Edwards, H. Worden, M. Luo, C. Rinsland, and W. McMillan : Carbon monoxide distributions from the IASI/METOP mission: evaluation with other space-borne remote sensors, *Atmos. Chem. Phys.*, 9, 8317–8330, doi:10.5194/acp-9-8317-2009, 2009. <sup>1415</sup>
- Gielen, C., M. Van Roozendael, F. Hendrick, G. Pinardi, T. Vlemmix, V. De Bock, H. De Backer, C. Fayt, C. Hermans, D. Gillotay, and P. Wang : A simple and versatile cloud-screening method for MAX-DOAS retrievals, *Atmos. Meas. Tech. Discuss.*, 7, 5883–5920, doi:10.5194/amtd-7-5883-2014, 2014. <sup>1420</sup>
- 1375 González Abad, G., X. Liu, K. Chance, H. Wang, T. P. Kurosu, and R. Suleiman : Updated Smithsonian Astrophysical Observatory Ozone Monitoring Instrument (SAO OMI) formaldehyde retrieval, *Atmos. Meas. Tech.*, 8, 19–32, doi:10.5194/amt-8-19-<sup>1425</sup>  
 1380 2015, 2015.
- Goodwin, J. W. L., A. G. Salway, T. P. Murrells, C. J. Dore, N. R. Passant, K. R. King, P. J. Coleman, M. M. Hobson, S. T. Pye, J. D. Watterson : UK Emissions of air pollutants 1970–1999, National Atmospheric Emissions Inventory Report,<sup>1430</sup>  
 1385 AEAT/ENV/R/0798, ISBN 1-85580-031 4., 2001, <http://uk-air.defra.gov.uk/reports/empire/naei/annreport/annrep99/appdx6.pdf>.
- Griffiths, P. R., and J. A. de Haseth : *Fourier Transform Infrared Spectrometry*, eds. John Wiley & Sons, Inc., Hoboken, New Jersey, 2007
- Guenther, A., T. Karl, P. Harley, C. Wiedinmyer, P. I. Palmer, and C. Geron: Estimates of global terrestrial isoprene emissions using MEGAN (Model of Emissions of Gases and Aerosols from Nature), *Atmos. Chem. Phys.*, 6, 3181–3210, 2006.
- Guenther, A., X. Jiang, C. L. Heald, T. Sakulyanontvittaya, T. Duhl, L. K. Emmons, and X. Wang: The Model of Emissions of Gases and Aerosols from Nature version 2.1 (MEGAN2.1): an extended and updated framework for modeling biogenic emissions, *Geosci. Model Dev.*, 5, 1471–1492, 2012.
- Hendrick, F., J.-F. Müller, K. Clémer, P. Wang, M. De Mazière, C. Fayt, C. Gielen, C. Hermans, J. Z. Ma, G. Pinardi, T. Stavrakou, T. Vlemmix, and M. Van Roozendael : Four years of ground-based MAX-DOAS observations of HONO and NO<sub>2</sub> in the Beijing area, *Atmos. Chem. Phys.*, 14, 765–781, 2014.
- Hewson, W., H. Bösch, M. P. Barkley, and I. De Smedt : Characterisation of GOME-2 formaldehyde retrieval sensitivity, *Atmos. Meas. Tech.*, 6, 371–386, doi:10.5194/amt-6-371-2013, 2013.
- Hönninger, G., G. von Friedeburg, and U. Platt : Multi axis differential optical absorption spectroscopy (MAX-DOAS), *Atmos. Chem. Phys.*, 4, 231–254, doi:10.5194/acp-4-231-2004, 2004.
- Huang, X., M. Xi, J. Li, and Y. Song : A high-resolution emission inventory of crop burning in fields in China based on MODIS thermal anomalies/fire products, *Atmos. Environ.*, 50, 9–15, 2012.
- Jenkin, M. E., T. P. Murrells, and N. R. Passant: The temporal dependence of ozone precursor emissions: estimation and application, AEA Technology, Report No. AEAT/R/ENV/0355 Issue 1, 2000.
- Junkermann, W. : On the distribution of formaldehyde in the western Po-Valley, Italy, during FORMAT 2002/2003, *Atmos. Chem. Phys.*, 9, 9187–9196, 2009.
- Kleipool, Q. L., M. R. Dobber, J. F. de Haan, and P. F. Levelt : Earth surface reflectance climatology from 3 years of OMI data, *J. Geophys. Res.*, 113(D18), D18308, doi:10.1029/2008JD010290, 2008.
- Krol, M., W. Peters, P. Hooghiemstra, M. George, C. Clerbaux, D. Hurtmans, D. McInerney, F. Sedano, P. Bergamaschi, M. El Hajj, J. W. Kaiser, D. Fisher, V. Yershov, and J.-P. Müller : How much CO was emitted by the 2010 fires around Moscow? *Atmos. Chem. Phys.*, 13, 4737–4747, doi:10.5194/acp-13-4737-2013, 2013.
- Kononov, I. B., M. Beekmann, I. N. Kuznetsova, A. Yurova, and A. M. Zvyagintsev : Atmospheric impacts of the 2010 Russian wildfires: integrating modelling and measurements of an extreme

- air pollution episode in the Moscow region, *Atmos. Chem. Phys.*, 11, 10031–10056, doi:10.5194/acp-11-10031-2011, 2011.
- Kurokawa, J., T. Ohara, T. Morikawa, S. Hanayama, J.-M. Greet,<sup>1480</sup>  
1435 T. Fukui, K. Kawashima, and H. Akimoto : Emissions of air pollutants and greenhouse gases over Asian regions during 2000–2008 : Regional Emission inventory in ASia (REAS) version 2, *Atmos. Chem. Phys.*, 13, 11019–11058, 2013.
- Langford, B., P. K. Misztal, E. Nemitz, B. Davison, C. Helfter,<sup>1485</sup>  
1440 T. A. M. Pugh, A. R. MacKenzie, S. F. Lim, and C. N. Hewitt : Fluxes and concentrations of volatile organic compounds from a South-East Asian tropical rainforest, *Atmos. Chem. Phys.*, 10, 8391–8412, 2010.
- Logan, J. A., M. J. Prather, S. C. Wofsy, and M. B. McElroy: Tro-<sup>1490</sup>  
1445 pospheric chemistry: A global perspective, *J. Geophys. Res.*, 86, 7210–7254, 1981.
- MacDonald, S. M., H. Oetjen, A. S. Mahajan, L. K. Whalley, P. M. Edwards, D. E. Heard, C. E. Jones, and J. M. C. Plane : DOAS measurements of formaldehyde and glyoxal above a south-east<sup>1495</sup>  
1450 Asian tropical rainforest, *Atmos. Chem. Phys.*, 12, 5949–5962, doi:10.5194/acp-12-5949-2012, 2012.
- Marais, E. A., D. J. Jacob, T. P. Kurosu, K. Chance, J. G. Murphy, C. Reeves, G. Mills, S. Casadio, D. B. Millet, M. P. Barkley, F. Paulot, and J. Mao : Isoprene emissions in Africa inferred from<sup>1500</sup>  
1455 OMI observations of formaldehyde columns, *Atmos. Chem. Phys.*, 12, 6219–6235, doi:10.5194/acp-12-6219-2012, 2012.
- Marais, E. A., D. J. Jacob, A. Guenther, K. Chance, T. P. Kurosu, J. G. Murphy, C. E. Reeves, and H. O. T. Pye : Improved model of isoprene emissions in Africa using Ozone Monitoring Instru-<sup>1505</sup>  
1460 ment (OMI) satellite observations of formaldehyde: implications for oxidants and particulate matter, *Atmos. Chem. Phys.*, 14, 7693–7703, doi:10.5194/acp-14-7693-2014, 2014.
- Marengo, J. A., C. Nobre, J. Tomasella, M. Oyama, G. Sampaio de Oliveira, R. de Oliveira, H. Camargo, L. Alves, and I. F. Brown <sup>1510</sup>  
1465 The Drought of Amazonia in 2005. *J. Climate* 21 (3): 495–516, doi:10.1175/2007JCLI1600.1, 2008.
- Marengo, J. A., J. Tomasella, L. M. Alves, W. R. Soares, and D. A. Rodriguez : The drought of 2010 in the context of historical droughts in the Amazon region, *Geophys. Res. Lett.*, 38 (12),<sup>1515</sup>  
1470 doi: 10.1029/2011GL047436, 2011.
- Martin, R. V, K. V. Chance, D. J. Jacob, T. P. Kurosu, R. J. D. Spurr, E. J. Bucsela, J. Gleason, P. I. Palmer, I. Bey, A. M. Fiore, Q. Li, R. M. Yantosca, and R. B. A. Koelemeijer : An improved retrieval of tropospheric nitrogen dioxide from GOME, *J. Geo-<sup>1520</sup>*  
1475 *phys. Res.*, 107(D20), doi:10.1029/2001JD001027, 2002.
- Millet, D. B., D. J. Jacob, S. Turquety, R. C. Hudman, S. Wu, A. Fried, J. Walega, B. G. Heikes, D. R. Blake, H. B. Singh, B. E. Anderson, and A. D. Clarke : Formaldehyde distribution over North America: Implications for satellite retrievals of formaldehyde columns and isoprene emission, *J. Geophys. Res.* 111, D24S02, doi:10.1029/2005JD006853, 2006.
- Millet, D. B., D. J. Jacob, K. F. Boersma, T. Fu, T. P. Kurosu, K. Chance, C. L. Heald, and A. Guenther : Spatial distribution of isoprene emissions from North America derived from formaldehyde columns measurements by the OMI satellite sensor, *J. Geophys. Res.*, 113, D02307, doi:10.1029/2007JD008950, 2008.
- Müller, J.-F., and T. Stavrakou: Inversion of CO and NOx emissions using the adjoint of the IMAGES model, *Atmos. Chem. Phys.*, 5, 1157–1186, 2005.
- Müller, J.-F., T. Stavrakou, S. Wallens. I. De Smedt, M. Van Roozendael, J. Rinne, B. Munger, A. Goldstein, and A. Guenther: Global isoprene emissions estimated using MEGAN, ECMWF analyses and a detailed canopy environmental model, *Atmos. Chem. Phys.*, 8, 1329–1341, 2008.
- Palmer, P. I., D. J. Jacob, A. Fiore, R. V. Martin, K. V. Chance, T. P. Kurosu, I. Bey, R. Yantosca : Air mass factor formulation for spectroscopic measurements from satellites: Application to formaldehyde retrievals from the Global Ozone Monitoring Experiment, *J. Geophys. Res.*, 106(D13), 14539–14550, doi:10.1029/2000JD900772, 2001.
- Palmer, P. I., D. J. Jacob, A. Fiore, K. V. Chance, R. V. Martin, T. P. Kurosu, I. Bey, R. Yantosca, A. Fiore, and Q. Li : Mapping isoprene emissions over North America using formaldehyde column observations from space, *J. Geophys. Res.*, 108(D6), 4180, doi:10.1029/2002JD002153, 2003.
- Palmer, P. I. D. S. Abbot, T.-M. Fu, D. J. Jacob, K. Chance, T. P. Kurosu, A. Guenther, C. Wiedinmyer, J. C. Stanton, M. J. Pilling, S. N. Pressley, B. Lamb, and A. L. Sumner, Quantifying the seasonal and interannual variability of North American isoprene emissions using satellite observations of the formaldehyde column, *J. Geophys. Res.* 111, D12315, doi:10.1029/2005JD006689, 2006.
- Peeters, J., T. L. Nguyen, and L. Vereecken: HOx radical regeneration in the oxidation of isoprene, *Phys. Chem. Chem. Phys.*, 11, 5935–5939, 2009.
- Peeters, J., and J.-F. Müller : HOx radical regeneration in isoprene oxidation via peroxy radical isomerisations. II: Experimental evidence and global impact, *Phys. Chem. Chem. Phys.*, 12(42), 14227–14235, doi:10.1039/C0CP00811G, 2010.
- Peeters, J., J.-F. Müller, T. Stavrakou, and S. V. Nguyen : Hydroxyl

- radical recycling in isoprene oxidation driven by hydrogen bond-<sup>1570</sup>  
<sup>1525</sup> ing and hydrogen tunneling : the upgraded LIM1 mechanism, *J. Phys. Chem. A*, 118 (38), 8625–8643, doi: 10.1021/jp5033146, 2014.
- Peters, E., F. Wittrock, K. Großmann, U. Frieß, A. Richter, and J. P. Burrows : Formaldehyde and nitrogen dioxide over the remote<sup>1575</sup>  
<sup>1530</sup> western Pacific Ocean: SCIAMACHY and GOME-2 validation using ship-based MAX-DOAS observations, *Atmos. Chem. Phys.*, 12, 11179–11197, doi:10.5194/acp-12-11179-2012, 2012.
- Pinardi, G., M. Van Roozendaal, N. Abuhassan, C. Adams, A. Cede, K. Clémer, C. Fayt, U. Friess, M. Gil, J. Herman, C. Hermans,<sup>1580</sup>  
<sup>1535</sup> F. Hendrick, H. Irie, A. Merlaud, M. Navarro Comas, E. Peters, A. J. M. Piters, O. Puentedura, A. Richter, A. Schönhardt, R. Shaiganfar, E. Spinei, K. Strong, H. Takashima, M. Vrekoussis, T. Wagner, F. Wittrock, and S. Yilmaz : MAX-DOAS formaldehyde slant column measurements during CINDI: intercompari-<sup>1585</sup>  
<sup>1540</sup> son and analysis improvement, *Atmos. Meas. Tech.*, 6(1), 167–185, doi:10.5194/amt-6-167-2013, 2013.
- Platt, U. and J. Stutz : Differential Absorption Spectroscopy, *Physics of Earth and Space Environments*, eds. Springer-Verlag Berlin, Heidelberg, doi:10.1007/978-3-540-75776-4, 2008. <sup>1590</sup>
- R'Honi, Y., L. Clarisse, C. Clerbaux, D. Hurtmans, V. Dufлот, S. Turquety, Y. Ngadi, and P-F. Coheur : Exceptional emissions of NH<sub>3</sub> and HCOOH in the 2010 Russian wildfires, *Atmos. Chem. Phys.*, 13, 4171–4181, doi:10.5194/acp-13-4171-2013, 2013.
- Richter, A., M. Begoin, A. Hilboll, and J. P. Burrows : An im-<sup>1595</sup>  
<sup>1550</sup> proved NO<sub>2</sub> retrieval for the GOME-2 satellite instrument, *Atmos. Meas. Tech.*, 4, 1147–1159, 2011.
- Roberts, G., M. J. Wooster, and E. Lagoudakis : Annual and diurnal african biomass burning temporal dynamics, *Biogeosciences*, 6, 849–866, 2009. <sup>1600</sup>
- Saide, P. E., J. Kim, C. H. Song, M. Choi, Y. Cheng, and G. R. Carmichael : Assimilation of next generation geostationary aerosol optical depth retrievals to improve air quality simulations, *Geophys. Res. Lett.*, 41, 9188–9196, doi:10.1002/2014GL062089, 2014. <sup>1605</sup>
- Sander, S. P., J. Abbatt, J. R. Barker, J. B. Burkholder, R. R. Friedl, D. M. Golden, R. E. Huie, C. E. Kolb, M. J. Kurylo, G. K. Moortgat, V. L. Orkin and P. H. Wine : Chemical Kinetics and Photochemical Data for Use in Atmospheric Studies, Evaluation No. 17, JPL Publication 10-6, Jet Propulsion Laboratory, Pasadena,<sup>1610</sup>  
<sup>1560</sup> 2011 <http://jpldataeval.jpl.nasa.gov>.
- Saunders, S. M., M. E. Jenkin, R. G. Derwent, and M. J. Pilling : Protocol for the development of the Master Chemical Mechanism, MCM v3 (Part A): tropospheric degradation of nonaromatic volatile organic compounds, *Atmos. Chem. Phys.*, 3, 161–<sup>1615</sup>
- 180, 2003.
- Schultz, M. G, A. Heil, J. J. Hoelzemann, A. Spessa, K. Thonicke, J. Goldammer, A. C. Held, J. M. Pereira : Global Emissions from Wildland Fires from 1960 to 2000, *Global Biogeochem. Cycles*, 22, GB2002, doi:10.1029/2007GB003031, 2008.
- Singh, H. B., W. H. Brune, J. H. Crawford, D. J. Jacob, and P. B. Russell : Overview of the summer 2004 Intercontinental Chemical Transport Experiment North America (INTEX-A), *J. Geophys. Res.*, 111(D6), D24S01, doi:10.1029/2006JD007905, 2006.
- Sofiev, M., T. Ermakova, and R. Vankevich : Evaluation of the smoke injection height from wild-land fires using remote sensing data, *Atmos. Phys. Chem.*, 12, 1995–2006, 2012.
- Sofiev, M., R. Vankevich, T. Ermakova, and J. Hakkarainen : Global mapping of maximum emission heights and resulting vertical profiles of wildfire emissions, *Atmos. Chem. Phys.*, 13, 7039–7052, 2013.
- Spurr, R. J. D. : LIDORT and VLIDORT: Linearized pseudo-spherical scalar and vector discrete ordinate radiative transfer models for use in remote sensing retrieval problems, in *Light Scattering Reviews*, edited by A. Kokhanovsky, pp. 229–271, Berlin, 2008.
- Stammes, P., M. Sneep, J. F. de Haan, J. P. Veefkind, P. Wang, and P. F. Levelt : Effective cloud fractions from the Ozone Monitoring Instrument: Theoretical framework and validation, *J. Geophys. Res.*, 113(D16), D16S38, doi:10.1029/2007JD008820, 2008.
- Stavrakou, T., J.-F. Müller, I. De Smedt, M. Van Roozendaal, G. van der Werf, L. Giglio, and A. Guenther : Evaluating the performance of pyrogenic and biogenic emission inventories against one decade of space-based formaldehyde columns, *Atmos. Chem. Phys.*, 9, 1037–1060, 2009a.
- Stavrakou, T., J.-F. Müller, I. De Smedt, M. Van Roozendaal, G. van der Werf, L. Giglio, and A. Guenther : Global emissions of non-methane hydrocarbons deduced from SCIAMACHY formaldehyde columns through 2003–2006, *Atmos. Chem. Phys.*, 9, 3663–3679, 2009b.
- Stavrakou, T., J. Peeters, and J.-F. Müller : Improved global modelling of HO<sub>x</sub> recycling in isoprene oxidation : evaluation against the GABRIEL and INTEX-A aircraft campaign measurements, *Atmos. Chem. Phys.*, 10, ~~9863–9878~~9863–9878, 2010.
- Stavrakou, T., J.-F. Müller, K.-F. Boersma, R.J. van der A, J. Kurokawa, T. Ohara, and Q. Zhang: Key chemical NO<sub>x</sub> sink uncertainties and how they influence top-down emissions of ni-

- trogen oxides, *Atmos. Chem. Phys.*, 13, 9057–9082, 2013.
- Stavrakou, T., J.-F. Müller, M. Bauwens, I. De Smedt, M. Van Roozendael, A. Guenther, M. Wild, and X. Xia : Isoprene emissions over Asia 1979–2012 : impact of climate and land use<sup>1620</sup> changes, *Atmos. Chem. Phys.*, 14, 4587–4605, 2014.
- Takahashi, H. G., H. Fujinami, T. Yasunari, and J. Matsumoto : Diurnal rainfall pattern observed by Tropical Rainfall Measuring Mission Precipitation Radar (TRMM-PR) around the Indochina peninsula, *J. Geophys. Res.*, 115, D07109,<sup>1625</sup> doi:10.1029/2009JD012155, 2010.
- van der Werf, G. R., J. T. Randerson, L. Giglio, G. J. Collatz, M. Mu, P. S. Kasibhatla, D. C. Morton, R. S. DeFries, Y. Jin, and T. T. van Leeuwen: Global fire emissions and the contribution of deforestation, savanna, forest, agricultural, and peat fires (1997–<sup>1630</sup> 2009), *Atmos. Chem. Phys.*, 10, 11707–11735, 2010.
- Valks, P. J. M., G. Pinardi, A. Richter, J. C. Lambert, N. Hao, D. Loyola, M. Van Roozendael, and S. Emmadi : Operational total and tropospheric NO<sub>2</sub> column retrieval for GOME-2, *Atmos. Meas. Tech.*, 4(7), 1491–1514, doi:10.5194/amt-4-1491-2011,<sup>1635</sup> 2011.
- Vigouroux, C., F. Hendrick, T. Stavrakou, B. Dils, I. De Smedt, C. Hermans, A. Merlaud, F. Scolas, C. Senten, G. Vanhaelewyn, S. Fally, M. Carleer, J.-M. Metzger, J.-F. Müller, M. Van Roozendael, and M. De Mazière : Ground-based FTIR and MAX-DOAS<sup>1640</sup> observations of formaldehyde at Réunion Island and comparisons with satellite and model data, *Atmos. Chem. Phys.*, 9(4), 15891–15957, doi:10.5194/acp-9-9523-2009, 2009.
- Vlemmix, T., F. Hendrick, G. Pinardi, I. De Smedt, C. Fayt, C. Hermans, A. PETERS, P. Levelt, and M. Van Roozendael : MAX-DOAS observations of aerosols, formaldehyde and nitrogen dioxide in the Beijing area: comparison of two profile retrieval approaches, *Atmos. Meas. Tech.*, 8, 941–963, doi:10.5194/amt-8-941-20157, 2015.
- Wang, P., P. Stammes, R. J. van der A, G. Pinardi, and M. Van Roozendael : FRESCO+: an improved O<sub>2</sub> A-band cloud retrieval algorithm for tropospheric trace gas retrievals, *Atmos. Chem. Phys.*, 8, 6565–6576, doi:10.5194/acp-8-6565-2008, 2008.
- Wiedinmyer, C., S. Akagi, R. J. Yokelson, L. K. Emmons, J. A. Al-Saadi, J. J. Orlando, A. J. Soja : The Fire INventory from NCAR (FINN): a high resolution global model to estimate the emissions from open burning, *Geosci. Model Dev.*, 4, 625–641,<sup>1655</sup> doi:10.5194/gmd-4-625-2011, 2011.
- Yamaji, K., J. Li, I. Uno, Y. Kanaya, H. Irie, M. Takigawa, Y. Komazaki, P. Pochanart, Y. Liu, H. Tanimoto, T. Ohara, X. Yan, Z. Wang, and H. Akimoto: Impact of open crop residual burning on air quality over Central Eastern China during the Mount Tai<sup>1660</sup> Experiment 2006 (MTX2006), *Atmos. Chem. Phys.*, 10, 7353–7368, 2010.
- Yurganov, L. N., V. Rakitin, A. Dzhola, T. August, E. Fokeeva, M. George, G. Gorchakov, E. Grechko, S. Hannon, A. Karpov, L. Ott, E. Semutnikova, R. Shumsky, and L. Strow : Satellite- and ground-based CO total column observations over 2010 Russian fires: accuracy of top-down estimates based on thermal IR satellite data, *Atmos. Chem. Phys.*, 11, 7925–7942, doi:10.5194/acp-11-7925-2011, 2011.

**Table 1.** ~~MCMv3.2 based short term yields (after 1 day) and final yields (after 60 days) of HCHO from Model simulations conducted to investigate the oxidation diurnal cycle of NMVOCs not explicitly considered in the IMAGES mechanism HCHO columns (Sect. The OH reaction rates at 298 K and the estimated emissions for the UK are also provided 3).~~

NMVOC	Molecular	$Y_{1d}$	$Y_{60d}$	OH reaction rate	Emission weight
	mol/mol	mol/mol	$\text{cm}^3 \text{molec.}^{-1} \text{s}^{-1}$	kt/yr	
Higher butane	58	0.280	2.033	$2.35 \cdot 10^{-12}$	151.11
alkanes-pentane	72	0.600	2.098	$4.00 \cdot 10^{-12}$	64.53
hexane	86	0.624	2.805	$5.45 \cdot 10^{-12}$	51.46
heptane	100	0.520	2.952	$7.02 \cdot 10^{-12}$	22.49
octane	114	0.505	2.976	$8.70 \cdot 10^{-12}$	15.08
nonane	128	0.541	3.128	$9.98 \cdot 10^{-12}$	6.03
decane	142	0.607	3.826	$1.12 \cdot 10^{-11}$	11.04
undecane	156	0.717	4.339	$1.29 \cdot 10^{-11}$	4.872
methylpropane	58	0.308	2.710	$2.18 \cdot 10^{-12}$	40.922
methylbutane	72	0.361	2.810	$3.70 \cdot 10^{-12}$	70.182
methylpentane	86	0.530	2.914	$5.30 \cdot 10^{-12}$	5.733
methylpentane	86	0.683	2.994	$5.40 \cdot 10^{-12}$	3.962
methylhexane	100	0.525	3.814	$6.86 \cdot 10^{-12}$	5.363
methylhexane	100	0.670	3.283	$7.15 \cdot 10^{-12}$	4.38
cyclohexane	86	0.541	1.615	$7.20 \cdot 10^{-12}$	4.31
Higher 1-butene	56	1.790	1.911	$3.14 \cdot 10^{-11}$	4.15
alkenes-2-methylpropene	56	1.117	2.890	$5.11 \cdot 10^{-11}$	11.371
pentene-70	1.852	2.157	3.14	$10^{-11}$	3.811
3-butadiene	54	1.644	1.711	$6.65 \cdot 10^{-11}$	6.19
Higher ethylbenzene	106	0.533	1.111	$7.00 \cdot 10^{-12}$	18.48
aromatics-1,2,3-trimethylbenzene	120	2.883	3.189	$3.27 \cdot 10^{-11}$	5.011
2,4-trimethylbenzene	120	2.883	3.189	$3.27 \cdot 10^{-11}$	5.011
Others-1-propanol	60	0.949	1.476	$5.82 \cdot 10^{-12}$	4.792
propanol	60	0.192	1.935	$5.09 \cdot 10^{-12}$	8.441
butanol	74	1.166	1.728	$8.48 \cdot 10^{-12}$	5.632
butanol	74	1.166	1.728	$8.48 \cdot 10^{-12}$	5.632

NBB

NDC

NDCBL

NDCC



**Table 2.** Performed ~~emission~~-flux inversions.

Name	Description
GOME-2	Use GOME-2 data
OMI	Use OMI data
OMI-DE	Doubled a priori errors on the emission fluxes
OMI-HE	Halved a priori errors on the emission fluxes
OMI-CF	Use only OMI data with cloud fraction < 0.2
OMI-IS	Ignore isomerization of isoprene peroxy radicals

**Table 3.** A priori and top-down VOC emissions (Tg/yr) by region. The emission inversions are defined in Table 2. The regions are defined as follows. North America : US and Canada, Southern America : Mexico, Central and South America, Northern (Southern) Africa : north (south) of the equator, Tropics : 25 S-25 N, Southeastern US : 25-38 N, 60-100 W, Amazonia : 14 S-10 N, 45-80 W, Indonesia : 10 S-6 N, 95-142.5 E, Indochina : 6-22 N, 97.5-110 E, Europe extends to Urals (55 E), FSU=Former Soviet Union.

<i>Biomass burning (TgVOC/yr)</i>	A priori	GOME-2	OMI	OMI-DE	OMI-HE	OMI-CF	OMI-IS
North America	5.3	3.6	3.3	5.3	2.9	4.6	3.2
Southern America	36.9	20.7	17.1	16.8	17.8	16.4	16.2
Amazonia	26.5	13.0	10.4	10.2	10.8	10.0	9.7
Northern Africa	14.9	8.6	8.8	8.8	9.2	9.7	8.1
Southern Africa	25.8	17.6	23.8	24.6	23.0	25.5	23.1
Indochina	6.2	4.6	5.3	5.6	4.7	5.6	5.0
Tropics	93.3	56.8	60.6	61.6	60.4	63.0	57.8
Extratropics	12.0	10.0	9.9	13.4	8.8	12.1	9.2
Global	105.4	67.0	70.5	74.9	69.1	75.1	67.1
<i>Isoprene (Tg/yr)</i>	A priori	GOME-2	OMI	OMI-DE	OMI-HE	OMI-CF	OMI-IS
Europe (excl. FSU)	3.8	3.3	3.8	3.7	3.4	3.9	3.7
Europe	7.4	6.9	8.2	8.8	7.7	8.6	8.1
North America	34.7	26.5	29.9	28.0	31.9	30.4	28.6
Southeastern US	14.5	8.9	10.8	9.8	12.2	11.3	9.9
Southern America	149.5	142.1	121.2	115.9	128.9	125.6	114.0
Amazonia	99.4	92.5	73.7	69.1	80.6	77.2	67.9
Northern Africa	50.6	45.3	43.7	40.4	46.8	44.7	41.5
Southern Africa	31.0	31.3	31.5	32.8	31.0	34.2	30.7
Indonesia	11.6	10.3	11.1	10.5	11.4	10.6	10.9
Indochina	7.6	7.1	7.5	7.3	7.5	7.4	7.3
Tropics	314.8	291.1	272.3	261.9	286.2	281.3	260.2
Extratropics	48.3	39.4	44.7	44.1	45.8	46.4	43.3
Global	363.1	330.5	317.0	305.9	332.1	327.8	303.5
<i>Anthropogenic (TgVOC/yr)</i>	A priori	GOME-2	OMI	OMI-DE	OMI-HE	OMI-CF	OMI-IS
Global	155.6	138.6	157.5	162.0	154.2	163.4	155.8